Stellar neutron capture cross sections of the Ba isotopes

F. Voss, K. Wisshak, K. Guber, and F. Käppeler
Kernforschungszentrum Karlsruhe, Institut für Kernphysik, Postfach 3640, D-76021 Karlsruhe, Germany

G. Reffo
ENEA, Laboratorio Dati Nucleari, Viale Ercolani 8, I-40138 Bologna, Italy
(Received 29 April 1994)

The neutron capture cross sections of ^{134}Ba, ^{135}Ba, ^{136}Ba, and ^{137}Ba were measured in the energy range from 5 to 225 keV at the Karlsruhe 3.75 MV Van de Graaff accelerator. Neutrons were produced via the ^{7}Li$(p,n)^{7}$Be reaction by bombarding metallic Li targets with a pulsed proton beam. Capture events were registered with the Karlsruhe 4π barium fluoride detector. The cross section ratios were determined with an overall uncertainty of ~3%, an improvement by factors of 5 to 8 compared to existing data. Severe discrepancies were found with respect to previous results. As a new possibility in time of flight experiments, isomeric cross section ratios could be determined for ^{135}Ba, ^{136}Ba, and ^{137}Ba. Maxwellian averaged neutron capture cross sections were calculated for thermal energies between kT = 10 keV and 100 keV. These stellar cross sections were used in an s-process analysis. For the s-only isotopes ^{134}Ba and ^{136}Ba the $N_s\langle\sigma\rangle$ ratio was determined to 0.875±0.025. Hence, a significant branching of the s-process path at ^{134}Cs can be claimed for the first time, in contrast to predictions from the classical approach. This branching yields information on the s-process temperature, indicating values around T_8 = 2. The new cross sections are also important for the interpretation of barium isotopic anomalies, which were recently discovered in SiC grains of carbonaceous chondrite meteorites. Together with the results from previous experiments on tellurium and samarium, a general improvement of the $N_s\langle\sigma\rangle$ systematics in the mass range A = 120–150 is achieved. This yields a more reliable separation of s- and r-process contributions for comparison with stellar observations, but reveals a 20% discrepancy with respect to the solar barium abundance.

PACS number(s): 25.40.Lw, 27.60.+j, 97.10.Cv, 98.80.Ft

I. INTRODUCTION

The main experimental program performed with the Karlsruhe 4π barium fluoride detector [1] is the accurate determination of neutron capture cross sections for nucleosynthesis studies related to s-process scenarios [2]. In this context, detailed analyses of branchings in the s-process path are of particular interest, since these branchings can be analyzed to derive information on the physical conditions during helium shell burning in Red Giant stars on the asymptotic branch (AGB). A first experiment on tellurium isotopes [3] confirmed the old prediction by Clayton *et al.* [4] that the product of neutron capture cross section $\langle\sigma\rangle$ and s-process abundance N_s is constant for neighboring isotopes with an uncertainty of only 1%. The validity of this *local approximation* strongly supports the idea to interpret (mostly small) deviations from this behavior as the result of branchings in the neutron capture path of the s process. In a previous experiment on samarium isotopes [5], a significant branching was observed and the analysis with the classical approach yielded a mean neutron density of $(3.8\pm0.6)\times10^{8}$ cm^{-3}, which is the most stringent value obtained so far.

The present investigation deals with the s process in the mass region around barium. The neutron capture path from xenon to barium (Fig. 1) shows that the two isotopes ^{134}Ba and ^{136}Ba are shielded from the r process by their stable xenon isobars. The unstable isotopes ^{133}Xe, ^{134}Cs, and ^{135}Cs are possible branching points due to the competition between neutron captures and β decays. The most significant of these branchings occurs at ^{134}Cs. Under laboratory conditions the 4^+ ground state of this isotope decays by allowed β decay to 4^+ states in the even even nucleus ^{134}Ba at excitation energies >1.4 MeV. This reduces the decay energy and yields a comparably long half life of 2.1 yr. However, at s-process temperatures, part of the ^{134}Cs nuclei are excited to the 3^+ level at 60 keV, allowing for β decays to the 2^+ level in ^{134}Ba at 0.6 MeV. The corresponding gain in decay energy leads to a considerable reduction of the half life, and, hence, to a temperature-dependent stellar decay rate of ^{134}Cs. Accordingly, analysis of the related branchings at A = 133–135 may yield information on the s-process temperature [6]. For this analysis, accurate neutron capture cross sections of the s-only barium isotopes are most important, since they allow to define the strength of these branchings.

A second problem, which requires accurate cross sections, is related to the large isotopic anomalies in barium, which were recently discovered in SiC grains, a very resistant fraction of carbonaceous chondrite meteorites [7–9]. If these anomalies are interpreted as being due to an admixture of pure s-process barium to the ordinary solar system abundances, the expected yields, N_s, have to be known reliably. Since the s-process yields are always inversely proportional to the stellar cross sections,

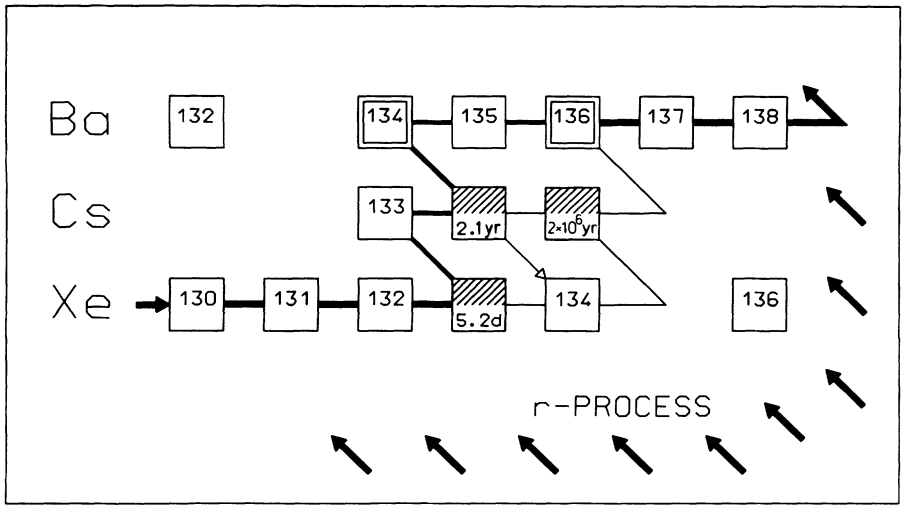

FIG. 1. The s-process path in the region of the barium isotopes with the s-only isotopes ^{134}Ba,^{136}Ba and the possible branching points ^{133}Xe, ^{134}Cs, and ^{135}Cs.

these are again the crucial nuclear physics information. These anomalies were studied via model calculations for the s-process in carbon stars by Gallino *et al.* [10]. The observed isotopic pattern could only be reproduced if the previously available cross sections [11] were significantly modified, the respective factors ranging from 1.0 to 2.2 for the different isotopes. The validity of this interpretation depends on whether these large differences can be verified by an improved experiment.

Another important aspect is related to astronomical studies of the surface composition of Red Giant stars, since barium can be considered as an s-process indicator. About 90% of the barium in nature is of s-process origin, while only ~10% are contributed by the r process. This s assignment allows one to study the enrichment of the stellar envelope with freshly produced s-process matter from the helium burning shell. Since europium is an almost pure r-process counterpart, variation of the Ba/Eu ratio with metallicity represents a critical test for galactic evolution models [12,13].

Last but not least, ^{136}Ba represents one of the normalization points of the $N_s\langle\sigma\rangle$ curve, together with ^{124}Te and ^{150}Sm. The accurate cross sections of these three isotopes allow for a significant improvement of the mean neutron exposure in the *main* s-process component, which is most sensitively defined in the mass range $A = 120$–150. Together with the improved cross sections of the other Te, Ba, and Sm isotopes, the r-process residuals can be updated as well. As pointed out by Meyer *et al.* [14], the mass range around the first r-process abundance peak is critical for r-process calculations. Therefore, better data are important in this region to reduce the respective uncertainties in the results of Ref. [2], which are presently used for comparison with r-process calculations.

The experimental status of the barium cross sections is unsatisfactory. There is only one experiment for all isotopes, but a number of publications with partly contradicting results. While the first series of publications [15–17] claimed uncertainties of 15–17% for the isotopes 134 to 137 and 20% for ^{138}Ba, these results were confused by revisions [18,19], where the ^{135}Ba cross section was changed by 55%. These discrepancies entered also into the evaluations of Bao and Käppeler [20] and of Beer, Voss, and Winters [11], respectively. In the keV range only one other data set was reported for ^{135}Ba [21], which confirmed the evaluation of Bao and Käppeler. From the data of Musgrove *et al.* [18], an experimental value for the branching factor,

$$(1 - f_n) \approx \frac{(N_s\langle\sigma\rangle)_{^{134}\mathrm{Ba}}}{(N_s\langle\sigma\rangle)_{^{136}\mathrm{Ba}}} = 0.99 \pm 0.21 \ ,$$

can be derived, which restricts a possible branching to $f_n \leq 20\%$. From analyses with the classical approach, a branching of only ~1% is expected [6].

In view of this situation, the neutron capture cross sections of ^{134}Ba, ^{135}Ba, ^{136}Ba, and ^{137}Ba were measured with the Karlsruhe 4π BaF_2 detector. Simultaneously, the very small cross section of neutron magic ^{138}Ba has been redetermined by Beer *et al.* [22] using the pulse height weighting technique. The experiments reported here were difficult for several reasons. First, the investigated cross sections are small, only 50 to 70 mb for ^{136}Ba and ^{137}Ba at 30 keV. Secondly, chemically stable $BaCO_3$ samples had to be used instead of the reactive elemental barium. Due to the light constituents in the compound, the scattering/capture ratio became as large as 300 to 400 at 30 keV, resulting in a significant background due to sample scattered neutrons. This background presents a severe problem, since scattered neutrons are captured in the barium isotopes of the scintillator, giving rise to the same sum energy signals in the detector as true capture events. This weakens the possibility of separating this background by selecting an appropriate sum energy window for determination of the cross section shape (Sec. III). Furthermore, nuclear level densities and, consequently, the multiplicities of the capture cascades are comparably low for these nearly neutron magic isotopes. Thus, the possibility of the 4π BaF_2 detector of separating true captures from natural background via the event multiplicity is reduced, too.

Nevertheless, the background from scattered neutrons

can still be separated efficiently due to the following reasons (for a detailed discussion see Ref. [1]): (i) About 90% of the scattered neutrons escape from the scintillator crystals without being captured. (ii) Neutrons that are eventually captured in the scintillator were scattered 20 times before on average. In view of the short primary flight path of 79 cm this implies a significant delay in time relative to the true capture events. Thus the respective events are shifted mostly to a time region, that is not used in data analysis. (iii) Captures of scattered neutrons are local events, activating predominantly the neighboring detector modules, whereas true capture events in the sample produce a uniform pattern in the 4π detector.

Therefore, only 70% of the observed effect had to be subtracted as background even in the unfavorable case of ^{136}Ba, where the ratio of total to capture cross section was about 360 at 30 keV [23].

The low multiplicities result in very hard capture gamma-ray spectra. Hence, experiments using the pulse height weighting technique become extremely difficult, since the complete setup including detector, surroundings, and the sample have to be modeled properly for obtaining the correct weighting function. This was not the case in the previous barium experiments and may explain the severe discrepancies found in the existing data.

The experiment and data analysis are described in Secs. II and III. In Sec. IV, the differential cross sections are presented together with the respective isomeric ratios, which could be determined for the first time in an experiment based on the detection of the prompt gamma-ray cascade. The uncertainties are discussed in Sec. V. The determination of stellar cross sections and the implications for astrophysics are given in Secs. VI and VII. A fully detailed description of the present experiment, data evaluation, calculation of correction factors, and the results of individual runs and evaluation methods can be found in Ref. [23].

II. EXPERIMENT

A. Experimental method

The neutron capture cross sections of the barium isotopes 134–137 were measured in the energy range from 3 to 225 keV using gold as a standard. Since the experimental method has been published in detail [1,3,5,24], only a more general description is given here, complemented with the specific features of the present measurement. Neutrons were produced via the ^{7}Li$(p,n)^7$Be reaction by bombarding metallic Li targets with the pulsed proton beam of the Karlsruhe 3.75 MV Van de Graaff accelerator. The neutron energy is determined by time of flight (TOF), the samples being located at a flight path of 78 cm. The important parameters of the accelerator are: pulse width <1 ns, repetition rate 250 kHz, and average beam current 1.5–2.5 μA. In different runs, the proton energies were adjusted 10, 30, and 100 keV above the threshold of the ^{7}Li$(p,n)^7$Be reaction at 1.881 MeV. In this way, continuous neutron spectra in the energy range of interest for s-process studies were obtained, ranging from 3 to 80 keV, 3 to 100 keV, and 3 to 200 keV, respectively. The use of different spectra allowed us to optimize the signal to background ratio in different neutron energy regions (Sec. III).

The signal to background ratio at a distinct energy E_n is dependent on the intensity of the neutron flux at E_n (which is proportional to the signal), and the integral neutron flux for energies larger than E_n (which is responsible for the background). At E_n = 30 keV, optimum conditions are obtained in the run with the lowest maximum neutron energy [23]. At energies below 10 keV, the run with 100 keV maximum neutron energy is more favorable due to the larger neutron flux. The run with 200 keV maximum neutron energy is necessary to determine the cross section above 100 keV.

The Karlsruhe 4π barium fluoride detector was used for the registration of capture gamma-ray cascades. This detector (a comprehensive description is given in Ref. [1]) consists of 42 hexagonal and pentagonal crystals forming a spherical shell of BaF_2 with 10 cm inner radius and 15 cm thickness. It is characterized by a resolution in gamma ray energy of 7% at 2.5 MeV, a time resolution of 500 ps, and a peak efficiency of 90% at 1 MeV. Capture events are registered with >95% probability.

In one run of the present experiment, an ADC system was used for data acquisition [25]. This system is based on CAMAC modules of type FERA (Le Croy). It allows us to store the gamma-ray energy and TOF information of each individual detector module that has fired in a particular event.

The purpose of the ADC system is fourfold. (i) It allows us to measure capture cascades and capture gamma-ray spectra directly. This information is necessary to determine the detector efficiency for capture events and had to be taken from theoretical calculations previously [24]. (ii) It offers a deeper understanding of the capture process, e.g., by determining angular or multiplicity distributions of capture gamma rays. (iii) It reduces significantly the recorded event rate by rejecting events in sum energy and TOF regions that are not needed for the evaluation of the cross section [5]. (iv) It allows us to improve the resolution in gamma-ray sum energy by offline corrections of the nonlinearity of individual detector modules.

The combination of a 4π BaF_2 detector with a Van de Graaff accelerator offers several advantages: The entire capture cascade is detected with good energy resolution. Thus, ambiguities in the detection efficiency due to different cascade multiplicities are avoided, and neutron capture events can be separated from gamma-ray background and from background due to capture of sample scattered neutrons by selecting events with the proper sum energy. The high granularity of the detector allows for a further separation of capture events and background by means of the recorded event multiplicity. The short primary flight path and the inner radius of the detector guarantee that a part of the TOF spectrum is completely undisturbed by background from sample scattered neutrons (Sec. III). This range with optimum signal to background ratio can be used to normalize the cross section. The high detection efficiency allows the

use of small samples avoiding large multiple scattering corrections. Finally, the $^7Li(p,n)^7Be$ reaction yields neutrons exactly and exclusively in the range of interest for s-process studies.

B. Samples

Isotopically enriched samples have been prepared from $BaCO_3$ powder, which has a lower scattering yield compared to the nitrate. Therefore, two batches of sample material had to be converted from nitrate to carbonate. The relevant parameters of the six samples are compiled in Table I. In addition to the four barium samples, a gold sample, a graphite sample, and an empty position in the sample changer frame were used in all runs. The respective sample masses of the barium isotopes were selected according to the expected cross sections in order to obtain similar capture yields in all cases. The yield of the gold sample was larger by a factor of 2. In this way the statistical uncertainty is dominated by the sample and not by the standard. Compared to the previous experiment by Musgrove *et al.* [16], the sample masses could be reduced by factors of 3–10. Accordingly, the sample related uncertainties for neutron multiple scattering and self-shielding corrections became significantly smaller.

For accurate cross section measurements the exact characterization of the samples can be a serious problem [26]. In the present experiment, however, the corresponding uncertainty is practically negligible since barium carbonate is chemically very stable and also not hygroscopic. This stability was verified by heating the pressed sample pellets to 300 °C without finding any change in weight. After the measurements, the weight of all samples could be perfectly reproduced as well.

Eventually, the samples were not only checked for contamination with water but also for possible deviations from the assumed stoichiometry. In a first analysis, part of the sample material was dissolved in diluted hydrochloric acid to a concentration of about 30 mg/ml. The barium content of this solution was determined via K-edge densitometry [27,28] as described in Ref. [5]. The standard solution for the calibration was prepared from natural barium carbonate, that was heated before to 300 °C. The measured barium concentrations agreed within the experimental uncertainty of 0.2% with that calculated for pure $BaCO_3$. A second batch of one of the samples was analyzed for its water content as described in Ref. [5], but only an upper limit for a possible contamination of 0.05% in weight was found.

The third step in characterizing the samples concerned the isotopic composition, which was redetermined at Karlsruhe together with natural barium as an independent check. The results are compared in Table II with the compositions certified by the suppliers. The agreement between the various data sets is quite satisfactory.

Though it was not necessary to encapsulate the samples in vacuum sealed cannings, they were covered with an 0.02 mm thick aluminum foil to avoid any losses of sample material. Accordingly, a bare aluminum canning was mounted in the "empty" position of the sample changer (Table I).

The diameter of all samples was 22 mm. As can be seen from Table I, some samples are comparably thick, resulting in neutron transmission values below 0.9 . Since reliable total cross sections of the barium isotopes were not available in literature, the spectra measured with the neutron monitor at 260 cm flight path could not be corrected for this effect. Instead, the TOF spectra taken with this detector were used for a rough determination of the total cross sections. Though the accuracy of this method is inferior to that obtained in a dedicated experiment, the derived total cross sections are sufficient for a reliable calculation of the multiple scattering corrections (Sec. III). Normalization of the spectra to equal neutron flux was performed by means of the second monitor detector located close to the neutron target.

C. Measurements

The samples were moved cyclically into the measuring position by a computer controlled sample changer. The data acquisition time per sample was about 10 min, a complete cycle lasting about 1.2 h. From each event, a 64 bit word was recorded on magnetic tape containing

TABLE I. Sample characteristics.

Sample[a]	Thickness		Weight[b]	Canning[c]	Impurity[d]	Neutron binding
	(mm)	(10^{-3} at./b)[e]	(g)	(mg)	(%)[f]	energy (MeV)
Au	0.25	1.5048	1.8709	75.7		6.513
Graphite	4.9	42.1544	3.1960	81.3		
^{134}Ba	1.8	1.7959	2.2053	75.7	<0.1	6.974
^{135}Ba	1.2	1.1168	1.3755	75.3	<0.1	9.107
^{136}Ba	5.1	5.2964	6.5564	81.4	<0.1	6.898
^{137}Ba	6.1	6.3918	7.9555	81.8	<0.1	8.611
Empty				75.6		

[a]All samples 22 mm in diameter.
[b]For barium samples: weight of $BaCO_3$.
[c]0.02 mm aluminum foil.
[d]Elements apart from carbon and oxygen.
[e]For barium samples: sum of all Ba isotopes.
[f]Percent of weight.

TABLE II. Isotopic compositions (%).

Sample	Isotope							Analysis
	^{130}Ba	^{132}Ba	^{134}Ba	^{135}Ba	^{136}Ba	^{137}Ba	^{138}Ba	
^{134}Ba	0.019	0.015	81.998	4.250	2.073	2.051	9.594	KfK
	<0.1	<0.1	82.1	4.21	2.04	2.04	9.6	ORNL
^{135}Ba	0.001	0.003	0.198	93.870	2.990	0.676	2.262	KfK
	<0.09	<0.09	0.16	94.00	2.87	0.64	2.33	GUS
^{136}Ba	0.002	0.003	0.078	0.972	92.677	1.812	4.456	KfK
	<0.03	<0.03	0.09	0.88	92.65	1.82	4.56	ORNL
^{137}Ba	0.000	0.001	0.023	0.074	0.312	82.250	17.340	KfK
	<0.05	<0.05	<0.05	0.05	0.26	82.20	17.49	GUS
Ba_{nat}	0.108	0.102	2.432	6.621	7.873	11.231	71.633	KfK

the sum energy and TOF information together with 42 bits indicating those detector modules that contributed. Three runs were performed using neutron spectra with 80, 100, and 200 keV maximum energies, respectively. To compensate for the reduced signal to background ratio caused by the larger background from scattered neutrons, the measuring time was increased by a factor of 2 compared to the previous measurements [3,5]. The data in the run with 100 keV maximum neutron energy were recorded with the ADC system. In the two runs using the conventional accquisition technique ~200 high density magnetic tapes containing roughly 35 Gbyte of information were recorded. With the ADC system, where the information per event is much larger, the total amount of data could be kept at ~20 Gbyte, since half of the background events were cut off by the preprocessing unit. The spectra of the two neutron monitor detectors were stored on magnetic disk as well.

III. DATA ANALYSIS

A. Total cross sections

The total cross sections of the barium isotopes were determined in the neutron energy range from 10 to 200 keV from the TOF spectra measured with the ^{6}Li glass detector at a flight path of 260 cm. The total cross sections and the related uncertainties were derived from these data as described in Ref. [5], and are listed in Table III. The carbon and oxygen cross sections required in this procedure were taken from a recent evaluation [Joint Evaluated File (JEF)] [29]. The total cross sections obtained for the carbon sample agree within ±0.5% with the JEF data. This represents a significant improvement compared to the results reported in Ref. [5], where systematic differences of 3% were found, and may be explained by the fact that in the previous experiment the sample diameter of 15 mm was just sufficient to shade the lithium glass scintillator. Thus, even a small misalignment of this detector could have caused the observed deviations, while such an effect was excluded in the present experiment.

The total gold cross sections are also improved compared to the last experiment [5], confirming again that these cross sections are significantly larger on average than the data given by McLane *et al.* [30]. This finding is supported by a recent measurement in Kiev [31]. The comparison of the experimental results with the ENDF/B-5 evaluation adopted in Ref. [30] is shown in Fig. 2.

B. Capture cross sections

The data analysis was carried out in analogy to the procedure described previously [3,5,24], and in detail in Ref. [23]. As far as the background subtraction is concerned, an essential feature of the present experimental method has to be emphasized. Capture events in the

TABLE III. The measured total cross sections (determined from the count rate of the ^{6}Li glass neutron monitor at 260 cm flight path).

Neutron energy (keV)	Total cross section (b)					
	^{134}Ba	^{135}Ba	^{136}Ba	^{137}Ba	^{12}C	^{197}Au
10 – 15	8.9	12.0	6.6	5.1	4.80	17.5
15 – 20	6.4	11.4	5.0	3.4	4.63	14.9
20 – 30	8.3	10.0	4.8	4.7	4.65	15.6
30 – 40	5.1	8.7	4.6	4.6	4.61	15.0
40 – 60	6.4	7.9	5.2	4.0	4.58	13.2
60 – 80	6.4	6.4	5.4	4.8	4.51	11.1
80 – 100	6.7	5.8	4.6	4.6	4.41	11.5
100 – 150	5.8	7.3	4.8	4.5	4.34	11.7
150 – 200	6.2	5.6	5.0	4.8	4.20	9.3
Uncertainty	7.4%	9.1%	3.6%	3.4%	0.5%	4.4%

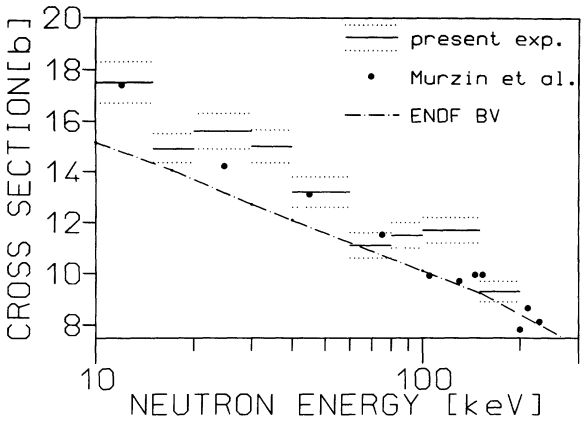

FIG. 2. The total cross section of gold in comparison to the results of a recent experiment and evaluation.

enriched barium samples are concentrated in the sum energy spectra at the binding energy of the respective isotope, whereas capture events due to scattered neutrons are distributed on all barium isotopes. For example, in the spectrum of an even isotope, such as ^{136}Ba with a typical binding energy of 6.9 MeV, the scattering background can be identified via the captures in the odd isotopes, which appear as a peak close to 9 MeV. In this way, the yield and time dependence of the scattering background can be well determined for all samples. The carbon sample is only used to determine the ratio of capture events in odd and even isotopes versus TOF. This possibility of defining the background from scattered neutrons is not available in experiments without energy resolution, but is important for avoiding systematic uncertainties. In this work, the corresponding uncertainty is dominated by statistics and is on the 1% level [23].

Sample-independent backgrounds were removed by subtraction of the spectra measured without sample. An additional constant background was determined at very long flight times, where no time-correlated events are expected. In the present measurement, the subtraction of this small time-independent component was more difficult than in previous experiments. The large scattering yields, especially from the ^{136}Ba and ^{137}Ba samples and from the thick graphite sample gave rise to an overlap with events from the previous pulse. As already mentioned, neutrons scattered from the sample into the detector are scattered many times in the scintillator before they are either captured or escape. Thus the respective background events are strongly delayed in time and may occur even more than 4 μsec after the proton pulse hits the target. Since the repetition rate of the accelerator is 250 kHz, there is a stop pulse in the TOF measurement every 4 μsec. An event delayed by 4.1 μsec will, therefore, be observed in the TOF spectrum at 0.1 μsec. Since this effect depends on the scattering yield from the sample and the integral neutron flux, it became observable for the first time with the $BaCO_3$ samples, especially in the run with 200 keV maximum neutron energy.

Therefore, the count rate in the TOF region around 3.9 μs (channels 1700–1900 in Fig. 3), where the constant background used to be determined, was not completely flat. Instead, the interval between the prompt gamma-ray peak and the onset of the capture events (channels 1500–1700) was chosen for normalization because it exhibits an additional delay of 200 ns. For the thickest samples, the count rates were not completely time independent even there so that this effect propagates into the TOF region used for cross section normalization (dashed area in Fig. 3). The correponding uncertainty is almost negligible in the run with 80 keV maximum neutron energy and most severe in the run with 200 keV, where the integral neutron flux is higher by about one order of magnitude. This systematic uncertainty in the normalization of the cross section is discussed in Sec. V. At larger TOF the uncertainty is rapidly decreasing. Actually, all cross section shapes obtained from runs with different maximum neutron energies agree within the respective statistical uncertainties.

In the correction for isotopic impurities, the contributions from ^{130}Ba, ^{132}Ba, and ^{138}Ba were neglected. For the light isotopes 130 and 132 this is justified because they contribute always less than 0.02% (Table II). The corrections for the ^{138}Ba impurities were relatively small because of the small cross section of that isotope. Therefore, the resulting uncertainties can be tolerated even for the 17% impurity in the ^{137}Ba sample (Sec. V). The largest correction for isotopic impurities was found for the ^{134}Ba sample, but also in this case it did not exceed 6% of the measured effect. The matrix for isotopic corrections is given in Table IV.

After the correction for isotopic impurities, the background due to capture of sample scattered neutrons was removed. In the present experiment, true captures in the samples are difficult to distinguish from background events due to capture of scattered neutrons in the scintillator, the only difference in the sum energy spectra being due to the different isotopic enrichments. The background subtraction is performed as in the previous ex-

TABLE IV. Matrix for the isotopic correction (%) [using the approximation that the abundances of ^{130}Ba=^{132}Ba=0, and that $\sigma(^{138}\text{Ba})=0$].

Corrected spectrum	Measured spectrum ^{134}Ba	^{135}Ba	^{136}Ba	^{137}Ba	Corrected sample Thickness (10^{-3} at./b)
^{134}Ba	100	−7.2423	−0.7065	−0.6773	1.4724
^{135}Ba	−0.1480	100	−0.6786	−0.1302	1.0479
^{136}Ba	−0.2713	−4.8827	100	−1.8166	4.9065
^{137}Ba	−0.0981	−0.4243	−0.4026	100	5.2568

periments [3,5,24], using the sum energy window around 9 MeV for the even isotopes; for the odd isotopes, the peak due to captures in ^{134}Ba and ^{136}Ba around 7 MeV was integrated. The possibility to calculate this normalization versus TOF is very important for the accuracy of the cross sections measured with the 4π BaF_2 detector.

The separation of true capture events from background due to scattered neutrons is complicated by the carbon and oxygen content of the sample material. The TOF spectra of the four barium samples are plotted in Fig. 3 (after projection of the two-dimensional data in the sum energy range around the binding energy; see below) together with the background due to scattered neutrons. The spectra are from the run with 100 keV maximum neutron energy. In this figure, three features are remarkable: (i) In contrast with previous measurements with the 4π BaF_2 detector [3,5,24], there is a significant background in the time interval used for the absolute normalization of the cross section (dashed area), resulting in a considerably reduced accuracy. (ii) The signal to background ratio deteriorates rapidly towards lower energies. Nevertheless, the data could be analyzed down to 3 keV, since the backgrounds are well known. However, the energy region below 5 and 10 keV was not used for the final evaluation of the stellar cross sections of the even and odd isotopes, respectively. (iii) The isotope ^{136}Ba requires special consideration since the resonances are completely resolved up to 15 keV neutron energy. Hence, the adopted procedure to evaluate average cross sections may not be adequate in this case, and fitting of the resonance parameters might be required. A corresponding study with the FANAC code [32] is in progress.

In view of the low signal to background ratio, the combination of runs with different neutron spectra was important. In this way, optimum conditions could be obtained in different energy regions. One finds that the signal to background ratios differ by more than a factor of 2 for different neutron spectra (see Ref. [23]). The difficult background situation is characterized by the fact that the ratio of total and capture cross sections reaches values up to ~400, which is a factor of 10 larger than for most isotopes measured so far. The fact that the previously developed procedures for treating this correction [3,5] worked successfully even in this extreme case confirms the validity of the background subtraction and justifies again that the related systematic uncertainties could be neglected in these earlier experiments. The uncertainties of the present data are discussed in Sec. V.

After background subtraction, the TOF spectra in Fig. 3 were used to determine the cross section shape.

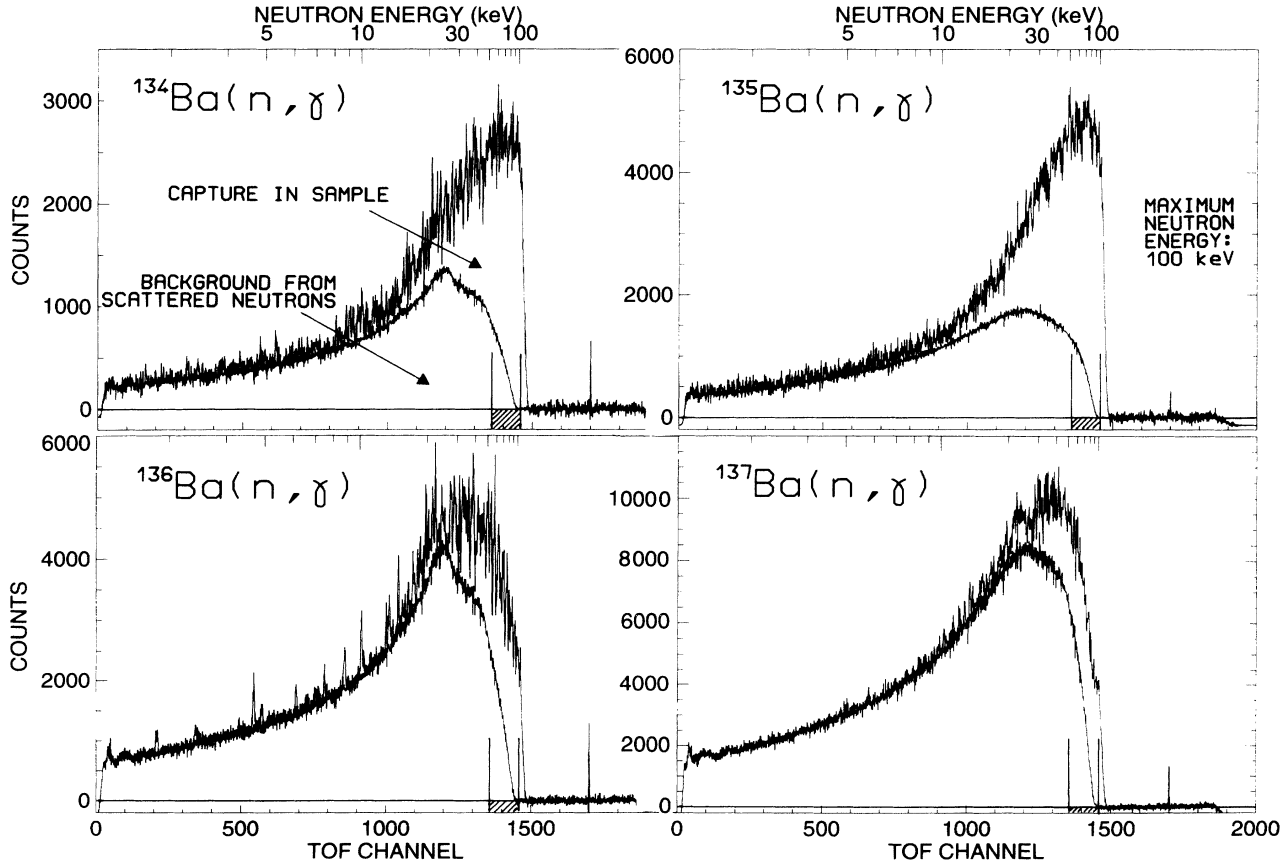

FIG. 3. TOF spectra measured with the barium samples in the run with 100 keV maximum neutron energy. The background due to sample scattered neutrons is shown separately. The region used for the absolute normalization of the cross section is indicated by hatched boxes. Note that the shape of the backgrounds due to sample scattered neutrons are different for the even and odd isotopes because they are derived from different regions in the sum energy spectrum (see text).

For normalization, the two-dimensional data were projected onto the sum energy axis using the TOF region of optimum signal to background ratio as indicated in Fig. 3 by dashed boxes. The resulting pulse height spectra are shown in Fig. 4 for the events with multiplicity >2. The spectra exhibit significant structures in the odd isotopes. The peaks in ^{135}Ba at 8.29 MeV and in ^{137}Ba at 7.17 MeV are due to the fact that nearly 80% of the capture cascades contain the $2^+ \rightarrow 0^+$ ground state transition in the respective compound nucleus (see inset of Fig. 4). Since the solid angle for detecting the corresponding gamma-ray lines at 0.82 MeV and 1.44 MeV is only 94%, the peak at the binding energy is shifted by this amount in the remaining 6% of all events.

The additional structures in the spectra of Fig. 4 are, however, due to isomeric states in the respective compound nuclei, which are also indicated in the insets. The half-lives of these isomers are between 0.8 μsec and 29 h, while the coincidence time for registration of capture γ-ray cascades is ~20 nsec. Thus, events feeding the isomer are registered with correspondingly lower sum energies. This is most clearly observed for ^{137}Ba, where the respective energy is 6.52 MeV. In ^{135}Ba, this effect is much weaker, yielding only an upper limit for the population of the isomer, while capture in ^{134}Ba feeds an isomer at 268 keV, which is too low to be resolved from the cascades to the ground state. But since ^{134}Ba and ^{136}Ba are very close in binding energy, the shape of the ^{134}Ba spectrum can be used to determine the population probability of the 662 keV isomer in ^{137}Ba. The structures in the spectra of Fig. 4 are statistically significant since they are observed in all three runs. This means that the probability for the population of isomeric states has been measured for the first time in a neutron TOF experiment.

The isomeric ratios

$$\mathrm{IR} = \frac{\text{partial cross section to isomer}}{\text{total } (n,\gamma) \text{ cross section}}$$

were determined in the TOF regions of optimum signal to background ratio. These regions are indicated by the dashed boxes in Fig. 3 and correspond to energy intervals 40–70 keV, 50–100 keV, and 70–150 keV. Within uncertainties, the obtained results do not exhibit any noticeable energy dependence: IR = <2%, 2.5±1%, and 3±1% for ^{135}Ba, ^{136}Ba, and ^{137}Ba, respectively.

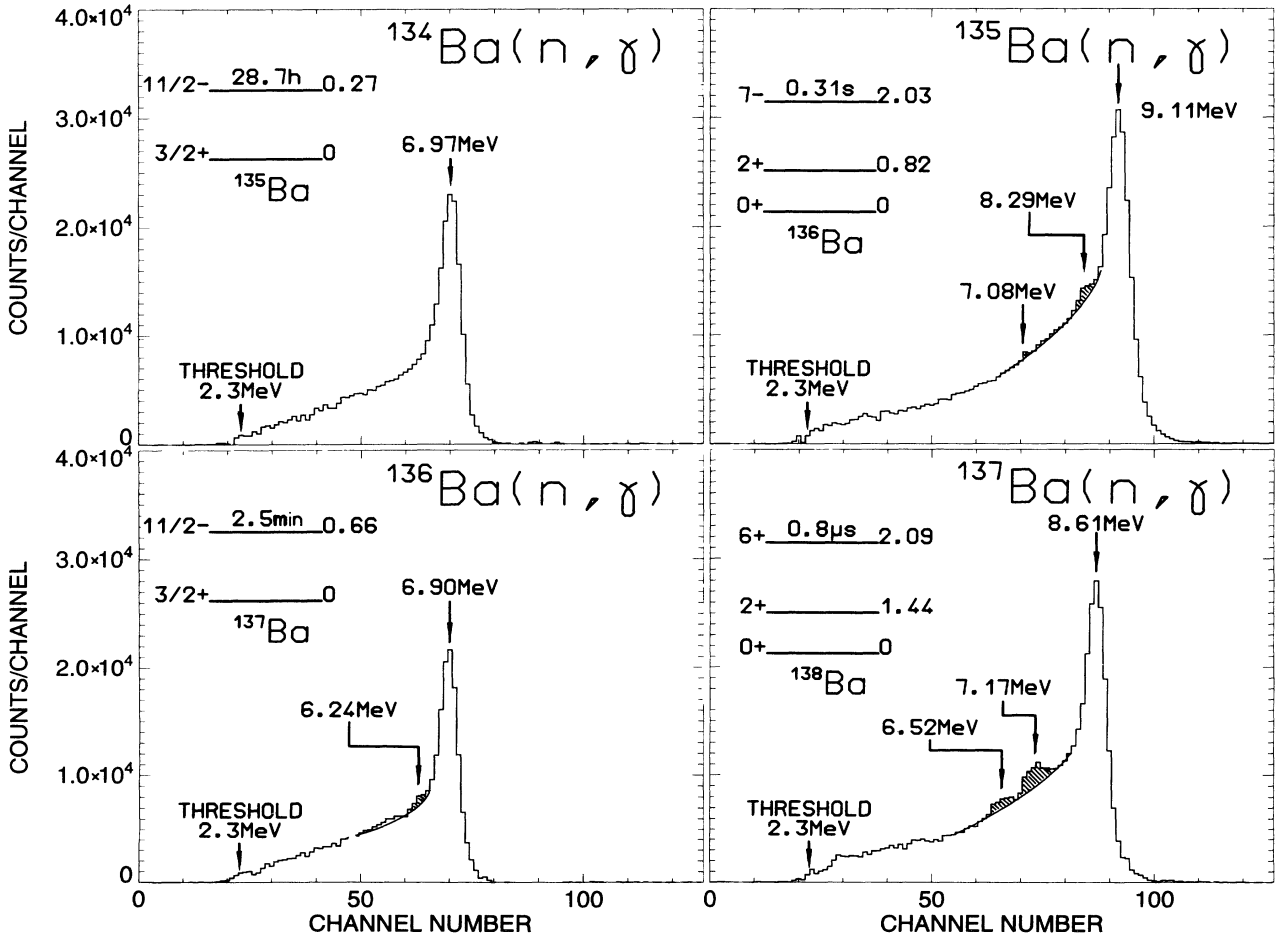

FIG. 4. Sum energy spectra of all isotopes measured in the run with 200 keV maximum neutron energy containing all events with multiplicity > 2. These spectra were obtained by projection of the two-dimensional spectra in the TOF region below the maximum neutron energy as indicated by hatched boxes in Fig. 3.

In Fig. 5, the sum energy spectra of the barium isotopes are shown for different multiplicities. (These multiplicities are determined by the number of detector modules contributing to an event. The true multiplicities are slightly smaller, because of cross talking effects.) In all cases, multiplicities ≥ 5 are observed for $\sim 40\%$ of the cascades, except for ^{136}Ba where the respective fraction is only $\sim 27\%$. This latter isotope shows an average multiplicity of only 2.3 due to the comparatively low binding energy and the low level density in ^{137}Ba (see below); accordingly, one finds a rather large fraction of events with multiplicity 1. The arrows in Fig. 5 indicate the range of sum energy channels that were combined to the TOF spectra in Fig. 3, from which the cross section shapes were determined.

The cross section ratio of isotope X relative to the gold standard is then

$$\frac{\sigma_i(X)}{\sigma_i(\mathrm{Au})} = \frac{Z_i(X)}{Z_i(\mathrm{Au})} \frac{\sum Z(\mathrm{Au})}{\sum Z(X)} \frac{\sum E(X)}{\sum E(\mathrm{Au})} \frac{m(\mathrm{Au})}{m(X)} F_1 F_2 \ . \quad (1)$$

In this expression, Z_i is the count rate in channel i of the TOF spectrum, $\sum Z$ is the TOF rate integrated over the interval used for normalization (Fig. 3), $\sum E$ is the total count rate in the sum energy spectrum for all multiplicities summed over the normalization interval (Fig. 4), and m is the sample thickness in atoms/barn. The factor $F_1 = [100 - f(\mathrm{Au})]/[100 - f(X)]$ corrects for the fraction of capture events f below the experimental threshold in sum energy, where X refers to the respective barium sample (Table V), and F_2 is the corresponding ratio of the multiple scattering and self-shielding corrections.

The fraction of unobserved capture events f and the correction factor F_1 were calculated as described in detail in Ref. [24]. The required input for this calculation are the individual neutron capture cascades and their relative contributions to the total capture cross section as well as the detector efficiency for monoenergetic gamma rays in the energy range up to 10 MeV.

Capture cascades and capture gamma-ray spectra of the involved isotopes were calculated according to the statistical and optical models [33]. Details are given in Ref. [23]. The average cascade multiplicities range from 2.3 to 3.7, and are significantly lower than for the previously investigated Te and Sm isotopes [3,5]. This difference reflects the proximity of the barium isotopes to the magic neutron configuration at $N = 82$.

The efficiency of the 4π BaF_2 detector for monoenergetic gamma-rays was calculated in Ref. [34] with different assumptions for multiple Compton events, resulting in an optimistic and a pessimistic estimate for the peak efficiency, SW(MAX) and SW(MIN). The corresponding data are listed in Ref. [24] and were since used to calculate the fraction of unobserved capture events. Recently, the gamma-ray efficiency of the 4π BaF_2 detector was determined experimentally [35] by measuring the line shapes for monoenergetic gamma rays in the energy range from 0.8 to 8.4 MeV. These gamma rays were produced by (p,γ) reactions on thin ^{26}Mg, ^{30}Si, and ^{34}S targets. In

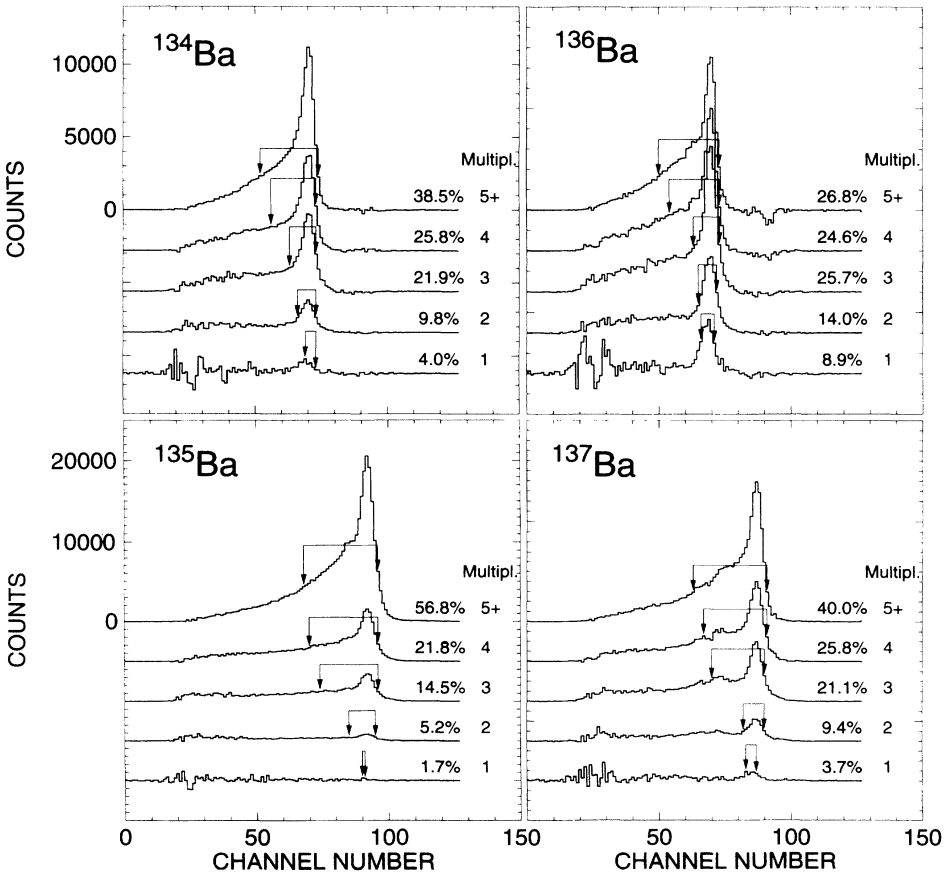

FIG. 5. Sum energy spectra of all barium isotopes in dependence of the detector multiplicity (the same data as shown in Fig. 4). The regions used to determine the cross section shape are indicated by arrows.

TABLE V. Fraction of undetected capture events, f (%), and the related correction factors (solid angle 94%, gamma-ray threshold 50 keV), F_1.

	Threshold in sum energy (MeV)				Assumption for
	2.0	2.2	2.3	2.5	gamma-ray efficiency
f(Au)	4.99			7.25	SW_{MAX}
$f(^{134}Ba)$	5.92			6.92	
$f(^{135}Ba)$	1.87			3.35	
$f(^{136}Ba)$	5.05			6.96	
$f(^{137}Ba)$	2.41			3.06	
f(Au)	5.78			8.35	SW_{MIN}
$f(^{134}Ba)$	6.30			7.91	
$f(^{135}Ba)$	2.41			3.64	
$f(^{136}Ba)$	5.73			7.61	
$f(^{137}Ba)$	2.74			4.10	
f(Au)	5.28			7.61	From experiment [35]
$f(^{134}Ba)$	5.35			6.89	
$f(^{135}Ba)$	1.83			2.95	
$f(^{136}Ba)$	5.41			6.76	
$f(^{137}Ba)$	2.24			3.53	
$F_1(^{134}Ba/Au)$	1.008			0.996	$(SW_{MAX}+SW_{MIN})/2$
$F_1(^{135}Ba/Au)$	0.967			0.955	
$F_1(^{136}Ba/Au)$	1.000			0.995	
$F_1(^{137}Ba/Au)$	0.971			0.956	
$F_1(^{134}Ba/Au)$	1.001	0.997	0.996	0.992	From experiment [35]
$F_1(^{135}Ba/Au)$	0.965	0.960	0.957	0.952	
$F_1(^{136}Ba/Au)$	1.001	0.997	0.995	0.991	
$F_1(^{137}Ba/Au)$	0.969	0.964	0.962	0.958	

these reactions, certain proton resonances decay predominantly by cascades with only two transitions. Replacing one of the BaF_2 modules by a Ge detector, and looking for BaF_2-Ge coincidences, two-dimensional spectra, E_γ(Ge) versus $E_\gamma(BaF_2)$ were recorded. The response of the 4π BaF_2 detector for monoenergetic gamma rays was then obtained by selecting those events, where the full energy of the complementary gamma ray is registered in the germanium detector.

Using seven (p,γ) resonances and an ^{88}Y source, the line shapes of 20 gamma transitions in the energy range from 0.843 to 8.392 MeV could be determined. Some of these spectra are shown in Ref. [23]. With these data, the calculations of the spectrum fractions f and of the correction factors F_1 were repeated (Table V). The respective results for F_1 being in very good agreement confirms once more the reliability of the 4π BaF_2 detector for precise cross section measurements.

The experimentally determined detector response will now be used in further cross section analysis. The calculated sum-energy spectra in Fig. 6 compare much better with the experimental spectra of Fig. 4 than was found in the previous experiments using the SW(MIN)/SW(MAX) approach [3,5]. The remaining difference is caused by the better energy resolution of the calculated spectra, and can be understood in terms of the different measuring times: the spectra with monoenergetic gamma rays were taken in a few hours, whereas a run in the capture experiment lasted for two months.

During the measurements, the threshold in sum energy was 2.2 MeV in run 1 and 2.3 MeV in runs 2 and 3. The resulting efficiency of the detector was 97% for the odd and 93% for the even isotopes. Since the barium samples and the gold standard are measured with the same detector, the final correction factors F_1 are very insensitive to the detector efficiency (Table V). For the even isotopes, which have binding energies similar to that of the gold standard, the efficiency correction is very small. For the odd isotopes, the efficiencies differ by $\leq$4%.

The correction for multiple scattering and self-shielding in the sample was calculated with the SESH code [36]. Details are given in Ref. [23]. In all calculations carbon and oxygen were considered according to the stoichiometry of $BaCO_3$. The correction factors F_2 are compiled in Table VI.

In view of the revised total cross sections for the gold standard (Sec. III), which are significantly higher than the before adopted ENDF/B-5 evaluation [30], the input parameters for this isotope were changed accordingly. In fact, the second parameter set discussed in Ref. [24] was used, which is based on the data given by Mughabghab *et al.* [37].

IV. RESULTS FOR THE NEUTRON CAPTURE CROSS SECTIONS

The neutron capture cross section ratios of the barium isotopes relative to ^{197}Au as obtained in individ-

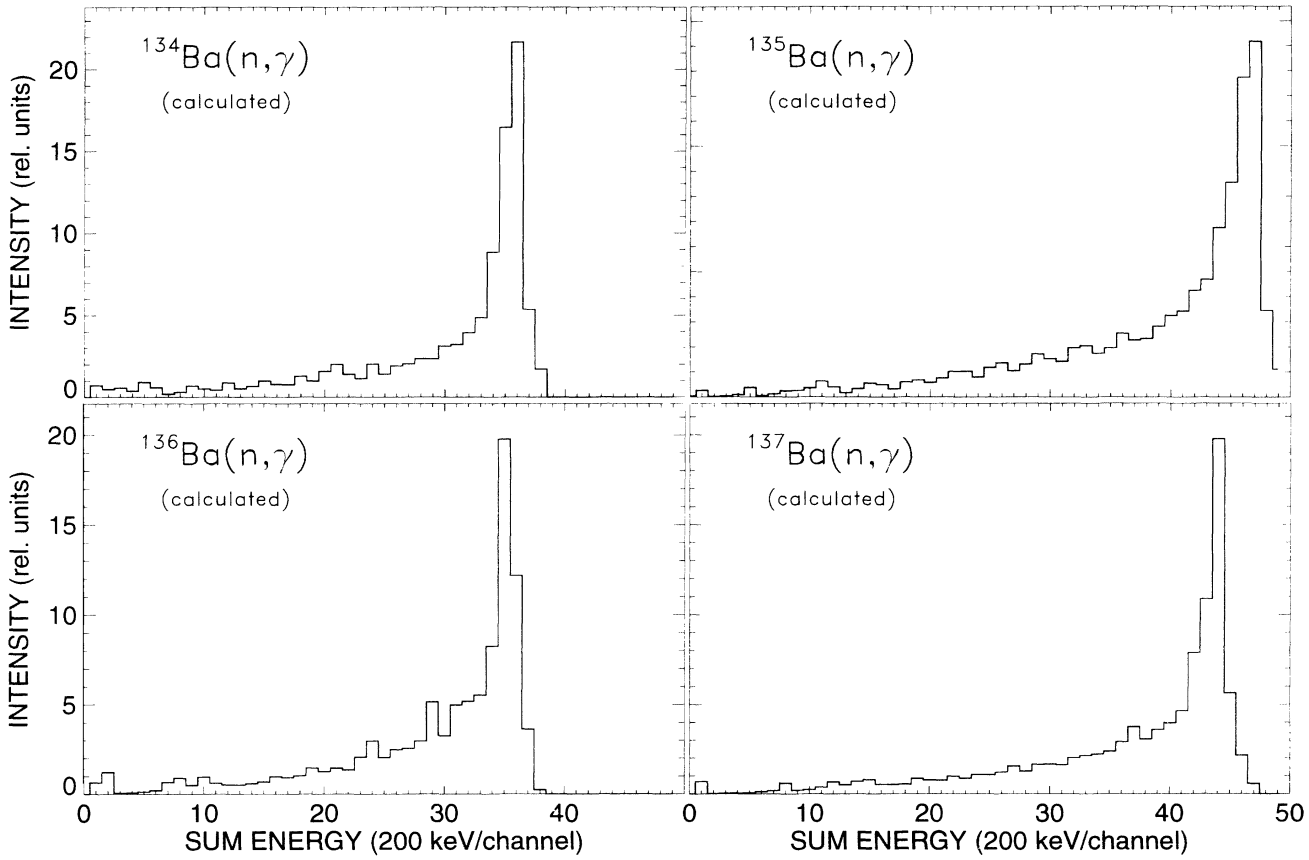

FIG. 6. Calculated sum energy spectra of the 4π BaF_2 detector as obtained using the measured line shape. These spectra were used to derive the correction F_1 for unobserved capture events.

TABLE VI. Correction factors for the cross section ratios, F_2 = MS(Au)/MS(X).

Energy range (keV)	F_2			
	^{134}Ba/Au	^{135}Ba/Au	^{136}Ba/Au	^{137}Ba/Au
3 – 5	1.031	1.002	1.128	1.065
5 – 7.5	1.013	1.004	1.086	1.040
7.5 – 10	1.009	1.004	1.058	1.024
10 – 12.5	1.008	1.007	1.047	1.017
12.5 – 15	1.005	1.006	1.039	1.012
15 – 20	1.001	1.004	1.027	1.005
20 – 25	0.998	1.003	1.017	1.000
25 – 30	0.995	1.002	1.009	0.996
30 – 40	0.992	1.000	1.000	0.991
40 – 50	0.990	0.999	0.992	0.987
50 – 60	0.988	0.997	0.987	0.984
60 – 80	0.985	0.995	0.983	0.980
80 – 100	0.983	0.993	0.981	0.977
100 – 120	0.983	0.992	0.981	0.975
120 – 150	0.982	0.991	0.980	0.973
150 – 175	0.981	0.990	0.980	0.972
175 – 200	0.980	0.989	0.979	0.971
200 – 225	0.980	0.988	0.978	0.970
Uncertainty (%)	0.4	0.3	0.4	0.4

ual runs are listed together with the respective statistical uncertainties in Ref. [23]. In the present experiment, there are significant differences in the results of individual runs. These discrepancies are due to the high scattering yield of the samples. As mentioned above, the subtraction of time-independent backgrounds was hampered due to the overlap from previous pulses, resulting in a significant background in the normalization interval (see Fig. 3). This background is difficult to determine because the respective count rates from the samples and the carbon sample exhibit strong differences in this TOF range (Sec. V). The results from the run with 80 keV maximum neutron energy being lower than the results from the other runs may indicate a systematic trend. On average, the individual cross section ratios deviate by 3.2% from their respective mean.

These systematic uncertainties affect only the barium spectra, but not the gold standard. One finds that the cross section ratios $\sigma(^{i}\mathrm{Ba})/\sigma(^{136}\mathrm{Ba})$ deviate from their means by 1.7% on average. Obviously, the cross section ratios of two barium isotopes are less affected, since the related corrections are partly cancelling each other. This behavior was considered in the evaluation of the uncertainties (Sec. V).

The mean values of the three runs are compiled in Table VII together with the statistical, systematic, and total uncertainties. The chosen energy bins are sufficiently fine to avoid systematic uncertainties in the calculation of the Maxwellian averaged cross sections (Sec. VI). The final uncertainties of the cross section ratios are ~3%,

TABLE VII. Final neutron capture cross section ratios of ^{134}Ba, ^{135}Ba, ^{136}Ba, and ^{137}Ba relative to ^{197}Au.

Energy interval[a]	$\frac{\sigma(^{134}\mathrm{Ba})}{\sigma(^{197}\mathrm{Au})}$	Uncertainty (%)			$\frac{\sigma(^{135}\mathrm{Ba})}{\sigma(^{197}\mathrm{Au})}$	Uncertainty (%)		
(keV)		stat	sys	tot		stat	sys	tot
3 – 5	0.2658	11.7			0.7861	10.1		
5 – 7.5	0.1994	8.2	3.1	8.8	0.6330	4.9		
7.5 – 10	0.3249	3.7	3.1	4.8	0.8773	2.7		
10 – 12.5	0.2809	3.1	3.1	4.4	0.6863	2.3	3.0	3.8
12.5 – 15	0.2213	3.5	3.1	4.7	0.7728	1.8	3.0	3.5
15 – 20	0.3378	1.4	3.1	3.4	0.8203	1.0	3.0	3.2
20 – 25	0.3452	1.2	3.1	3.3	0.9520	0.8	3.0	3.1
25 – 30	0.2773	1.1	3.1	3.3	0.8766	0.7	3.0	3.1
30 – 40	0.3318	0.7	3.1	3.2	0.8566	0.5	3.0	3.0
40 – 50	0.3101	0.7	3.1	3.2	0.8807	0.5	3.0	3.0
50 – 60	0.3369	0.7	3.1	3.2	0.8385	0.5	3.0	3.0
60 – 80	0.3268	0.5	3.1	3.1	0.7795	0.4	3.0	3.0
80 – 100	0.3510	0.6	3.1	3.2	0.7718	0.4	3.0	3.0
100 – 120	0.3398	0.6	3.1	3.2	0.7332	0.5	3.0	3.0
120 – 150	0.3252	0.8	3.1	3.2	0.7033	0.6	3.0	3.1
150 – 175	0.3326	0.9	3.1	3.2	0.6863	0.7	3.0	3.1
175 – 200	0.3295	1.0	3.1	3.3	0.6754	0.8	3.0	3.1
200 – 225	0.3152	1.7	3.1	3.5	0.6648	1.4	3.0	3.3

Energy interval[a]	$\frac{\sigma(^{136}\mathrm{Ba})}{\sigma(^{197}\mathrm{Au})}$	Uncertainty (%)			$\frac{\sigma(^{137}\mathrm{Ba})}{\sigma(^{197}\mathrm{Au})}$	Uncertainty (%)		
(keV)		stat	sys	tot		stat	sys	tot
3 – 5	0.1675	8.2			0.4423	16.5		
5 – 7.5	0.0958	7.5	3.2	8.2	0.1039	10.3		
7.5 – 10	0.0844	6.1	3.2	6.9	0.1310	4.7		
10 – 12.5	0.0852	4.4	3.2	5.4	0.1142	3.9	3.2	5.0
12.5 – 15	0.1224	2.9	3.2	4.3	0.1265	3.4	3.2	4.7
15 – 20	0.1344	1.6	3.2	3.6	0.1204	2.0	3.2	3.8
20 – 25	0.1196	1.6	3.2	3.6	0.1754	1.2	3.2	3.4
25 – 30	0.0925	1.5	3.2	3.5	0.1200	1.3	3.2	3.5
30 – 40	0.1168	0.8	3.2	3.3	0.1530	0.7	3.2	3.3
40 – 50	0.0982	0.9	3.2	3.3	0.1450	0.7	3.2	3.3
50 – 60	0.1208	0.8	3.2	3.3	0.1457	0.7	3.2	3.3
60 – 80	0.1080	0.6	3.2	3.3	0.1415	0.5	3.2	3.2
80 – 100	0.1164	0.7	3.2	3.3	0.1400	0.6	3.2	3.3
100 – 120	0.1137	0.7	3.2	3.3	0.1393	0.6	3.2	3.3
120 – 150	0.1080	1.0	3.2	3.4	0.1194	0.9	3.2	3.3
150 – 175	0.1028	1.1	3.2	3.4	0.1280	0.9	3.2	3.3
175 – 200	0.1092	1.1	3.2	3.4	0.1201	1.0	3.2	3.4
200 – 225	0.1077	1.8	3.2	3.7	0.1223	1.6	3.2	3.6

[a]As used for calculating the Maxwellian averaged cross sections.

at least 5 times smaller than obtained previously [16,17]. However, the 1% accuracy reported for the first results with the 4π BaF_2 detector [3,5] could not be met due to the background problems characteristic for the barium isotopes.

The experimental ratios were converted into cross sections by using the gold cross section of Macklin [38] after normalization by a factor of 0.989 to the absolute value of Ratynski and Käppeler [39] (Table VIII). The uncertainties of these data can be obtained by adding the 1.5% uncertainty of the standard to the uncertainties of the respective cross section ratios.

The present results can be compared to the data of Musgrove *et al.* [18]. In the energy range of interest between 30 and 100 keV, these data exhibit uncertainties of 15, 17, 25, and 17% for ^{134}Ba, ^{135}Ba, ^{136}Ba, and ^{137}Ba, and differ from the present results by factors 1.42, 1.08, 1.25, and 0.83, respectively. Except for ^{134}Ba, these differences are consistent with the quoted uncertainties, but seem to confirm a trend that was already noted in case of the samarium isotopes [5]. Before 1988, the weighting functions in experiments with total energy detectors did not consider the influence of detector cannings and the surrounding setup. In this way, the weight for high gamma-ray energies was consistently overestimated [40], leading to systematic uncertainties, whenever the capture gamma-ray spectra of the sample differed from that of the respective standard. The cross section ratio was overestimated, if the spectrum of the sample is harder than that of the standard, and underestimated, if it is softer. The spectra of both even barium isotopes being harder than that of gold [24], would explain the larger cross sections in the previous measurement. For the odd barium isotopes this effect is less pronounced since their spectra are rather similar to that of gold. This discussion holds also for the ^{135}Ba data of Mizumoto *et al.* [21], which are in agreement with those of Musgrove *et al.* [18].

For the even isotopes there are no significant differences in the cross section shapes down to 5 keV neutron energy, though the cross sections of Musgrove *et al.* [18] were determined from isolated resonances (in the energy range from 5 to 10 keV for ^{134}Ba and from 5 to 35 keV for ^{136}Ba), whereas our data were calculated by averaging the observed capture yields directly. This agreement confirms the background correction applied to the present data. In particular, the low energy range of the ^{136}Ba cross section (see Fig. 3), where only a few resonances are observed, would be extremely sensitive to a systematic uncertainty in the background subtraction. In order to exclude any remaining systematic effect, it is planned to deduce the resonance parameters for the isolated resonances in ^{136}Ba from the present data as well.

For the odd isotopes, deviations in the cross section shapes are observed below 10 keV. As discussed in Ref. [3], background subtraction at low energies is problematic, since the lines at 7 MeV had to be integrated in the pulse height spectra. Therefore, the data below 10 keV were not used in the calculation of stellar cross sections. The very uncertain results in the energy range from 3 to 5 keV were only included in Table VII to demonstrate that they show a reasonable trend despite the extremely poor signal to background ratio in the TOF spectra.

V. DISCUSSION OF UNCERTAINTIES

The determination of statistical and systematic uncertainties in measurements with the 4 π BaF_2 detector has been described in Refs. [3] and [24]. The following discussion concentrates on the particular aspects of the present experiment on the barium isotopes. The various uncertainties are compiled in Table IX.

In contrast to previous experiments [3,5,24], the large

TABLE VIII. Neutron capture cross sections of ^{134}Ba, ^{135}Ba, ^{136}Ba, and ^{137}Ba.

Energy interval[a] (keV)	$\sigma(^{197}Au)$[b] (mb)	$\sigma(^{134}Ba)$ (mb)	$\sigma(^{135}Ba)$ (mb)	$\sigma(^{136}Ba)$ (mb)	$\sigma(^{137}Ba)$ (mb)
5 – 7.5	1726.7	344.3		165.4	
7.5 – 10	1215.7	395.0		102.6	
10 – 12.5	1066.7	299.6	732.1	90.9	121.9
12.5 – 15	878.0	194.3	678.5	107.4	111.1
15 – 20	738.8	249.6	606.0	99.3	89.0
20 – 25	600.0	207.1	571.2	71.8	105.3
25 – 30	570.8	158.3	500.4	52.8	68.5
30 – 40	500.4	166.1	428.6	58.5	76.6
40 – 50	433.3	134.4	381.6	42.5	62.8
50 – 60	389.6	131.3	326.7	47.1	56.8
60 – 80	349.4	114.2	272.3	37.8	49.4
80 – 100	298.3	104.7	230.2	34.7	41.8
100 – 120	290.1	98.6	212.7	33.0	40.4
120 – 150	274.1	89.1	192.8	29.6	32.7
150 – 175	263.7	87.7	180.9	27.1	33.7
175 – 200	252.6	83.2	170.6	27.6	30.3
200 – 225	248.5	78.3	165.2	26.8	30.4

[a]As used for calculating the Maxwellian averaged cross sections.
[b]Based on the ^{197}Au data from literature [38,39].

TABLE IX. Systematic uncertainties (%).

Background subtraction in normalization	
Cross section ratio ^{x}Ba/Au	3.0
Cross section ratio ^{x}Ba/^{y}Ba	1.5
Flight path	0.1
Neutron flux normalization	0.1
Sample mass	0.1
Isotopic impurities (^{134}Ba/^{135}Ba/^{136}Ba/^{137}Ba samples)	0.2/0.1/0.3/1.0
Multiple scattering and self-shielding ratios	
Cross section ratio Ba/Au, ^{134}Ba/^{135}Ba/^{136}Ba/^{137}Ba samples	0.4/0.3/0.4/0.4
Cross section ratio ^{134}Ba/^{136}Ba	0.4
Undetected events	
Cross section ratio Ba/Au, ^{134}Ba/^{135}Ba/^{136}Ba/^{137}Ba samples	0.6/0.4/1.0/0.4
Cross section ratio ^{134}Ba/^{136}Ba	1.0
Total systematic uncertainties	
$\sigma(^{134}\mathrm{Ba})/\sigma(\mathrm{Au})$	3.1
$\sigma(^{135}\mathrm{Ba})/\sigma(\mathrm{Au})$	3.0
$\sigma(^{136}\mathrm{Ba})/\sigma(\mathrm{Au})$	3.2
$\sigma(^{137}\mathrm{Ba})/\sigma(\mathrm{Au})$	3.2
$\sigma(^{134}\mathrm{Ba})/\sigma(^{136}\mathrm{Ba})$	1.9

scattering yields of the barium samples and the fact that discrimination of the corresponding backgrounds was hampered by the barium content of the scintillator resulted in significantly reduced signal to background ratios. Therefore, the related systematic uncertainties were no longer negligible. The 4 μs interval between the accelerator pulses was not completely sufficient to exclude TOF overlap from previous pulses. Hence, the count rate in the TOF region used for the determination of time-independent backgrounds (e.g., channels 1500 to 1690 in Fig. 3) was still affected by a small time-dependent component. This gives rise to a systematic uncertainty in the normalization interval close to this region (see Fig. 3).

In addition, the normalization of the scattering correction is strongly TOF dependent in this critical interval, leading to a systematic uncertainty in the normalization of the cross section. As discussed above, the ^{136}Ba cross section in the region of resolved resonances provides a sensitive test of this correction. Since the observed scatter in the data of individual runs at low energies (above 5 keV for the even and above 10 keV for the odd isotopes) is fully compatible with the statistical uncertainties, a systematic uncertainty for the cross section shape could again be excluded. In the range from 30 to 80 keV, however, the data show statistically significant discrepancies in the absolute normalization. The corresponding systematic uncertainty affects mainly the cross section ratio relative to gold, since this problem occurs only for the barium isotopes. Actually, the average deviation from the respective mean suggested a systematic uncertainty of 3.0% for the cross section ratios relative to gold. For the ratio of two barium cross section, e.g., for the astrophysically important ratio $\sigma(^{134}\mathrm{Ba})/\sigma(^{136}\mathrm{Ba})$, this systematic uncertainty reduces to 1.5%, since both isotopes are affected in a similar way.

This normalization problem dominates the total systematic uncertainty. All other uncertainties are comparably small, and are in most cases equivalent to the uncertainties discussed in Ref. [5]. The differences in the actual values listed in Table IX refer to the following points. The uncertainty due to the correction for equal neutron flux could be reduced due to the larger number of measuring cycles. Also the sample masses were better defined, since there were no problems with water absorption in the barium carbonate. The uncertainty of the isotopic correction is dominated by the fact that ^{138}Ba was neglected in our data analysis. With the new ^{138}Ba cross section [22] and the isotopic abundances of Table II, a sizable uncertainty of 1% was found for ^{137}Ba only (Table IX). In fact, there are no indications for ^{138}Ba captures at 4.9 MeV in the spectra of Fig. 4. The uncertainties of the multiple scattering corrections are slightly larger than reported previously because of the larger samples used in the present experiment.

The correction for unobserved capture events needs special consideration. On one hand, the use of experimentally determined line shapes for monoenergetic gamma rays certainly improved the reliability of the correction, but on the other hand, the low multiplicities of the barium capture cascades produced the problem that the calculations were slightly dependent on the random numbers in the Monte Carlo simulation of the effective solid angle.

VI. MAXWELLIAN AVERAGED CROSS SECTIONS

Maxwellian averaged cross sections were calculated in the same way as described in Refs. [3] and [24]. The neutron energy range from 0 to 700 keV was divided into three intervals according to the origin of the adopted

TABLE X. Maxwellian averaged neutron capture cross sections of ^{134}Ba, ^{135}Ba, ^{136}Ba, and ^{137}Ba for thermal energies from 10 to 100 keV. (The 1.5% uncertainty of the gold standard is not included here, since it cancels out in most applications of relevance for nuclear astrophysics.)

kT (keV)	^{134}Ba (mb)	^{135}Ba (mb)	^{136}Ba (mb)	^{137}Ba (mb)
10	310.7±12.3	845.9±46.4	114.9±6.5	137.7±10.5
12	281.4±10.4	763.9±37.4	103.5±5.2	124.6±8.2
20	215.2±7.1	572.6±21.3	77.4±3.0	95.0±4.3
25	192.5±6.2	504.6±17.4	68.4±2.5	84.5±3.4
30	176.3±5.6	455.0±15.0	62.0±2.1	76.9±2.9
40	154.6±4.9	386.7±12.2	53.5±1.8	66.2±2.3
50	140.5±4.4	341.7±10.6	48.1±1.6	59.1±2.0
52	138.2±4.3	334.4±10.3	47.3±1.6	58.0±1.9
60	130.5±4.1	309.5±9.5	44.4±1.5	54.0±1.8
70	123.1±3.9	285.3±8.7	41.7±1.4	50.0±1.6
80	117.3±3.7	265.9±8.2	39.6±1.3	46.9±1.5
90	112.5±3.6	250.0±7.7	37.9±1.3	44.3±1.5
100	108.4±3.6	236.7±7.4	36.6±1.2	42.2±1.4

cross sections. The respective contributions I_x are given in Ref. [23]. The main contributions were obtained from the cross sections of the present experiment (Table VIII). The energy bins of these data were chosen sufficiently fine to exclude systematic uncertainties that may result from a coarse energy grid.

The contributions I_1 from the energy range from 0 to 5 keV for the even and from 0 to 10 keV for the odd isotopes was determined in two different ways. First, the cross section shapes from statistical model calculations were fitted at high energies to the present results and at low energies to the data that were calculated from resonance parameters [37]. In a second calculation, the cross sections of the Joint Evaluated File [29] were normalized to the present experiment in the region between 10 to 20 keV. Though the respective normalization factors were ranging from 1.20 to 1.42, the cross section shapes were found in good agreement between both data sets. For the adopted contributions the results from both calculations were averaged. The quoted uncertainty of 10–20% corresponding to the respective differences includes the systematic uncertainty of this component.

The energy interval from 225 to 700 keV contributes only very little to the Maxwellian average at typical s-process temperatures. There, the JEF data [29] were normalized to the present results between 100 to 200 keV. The uncertainties were calculated under the assumption that the uncertainty of the normalized cross sections increases from 2% at 225 keV to 10% at 700 keV.

The uncertainties of the Maxwellian averaged cross sections in Table X do not contain the 1.5% uncertainty of the gold standard since it cancels out in most applications of relevance for s-process studies (Sec. VII). They are dominated by the systematic contributions.

In calculating ratios of two barium cross sections, one must consider that the uncertainties given in Table X are strongly correlated and should, therefore, not be added in quadrature. For example, the statistical uncertainties of the cross section ratios are partly determined by the respective gold count rates [Z_i(Au), $\sum Z$(Au), $\sum E$(Au) in Eq. (1)], which cancel out in the cross section ratio of two barium isotopes. As discussed in Sec. V, the systematic uncertainties of such cross section ratios are significantly smaller (Table IX). The proper uncertainty of the ratio of Maxwellian averaged cross sections of two barium isotopes was evaluated explicitly for the s-only isotopes ^{134}Ba and ^{136}Ba, and is given in Table XI.

The present results at kT = 30 keV are eventually compared in Table XII with the data given in the compilations of Bao and Käppeler [20] and of Beer, Voss, and Winters [11]. Significant differences are found for the isotopes ^{134}Ba and ^{137}Ba. The low value for ^{135}Ba given in Ref. [11], which is based on Refs. [15] and [17], is completely ruled out by the present data. On average, the uncertainties have been reduced by a factor of 5.

Stellar enhancement effects on the investigated Maxwellian averaged cross sections are negligible according to statistical model calculations [41,42]. This means that excited nuclear states are not sufficiently populated in these isotopes at s-process temperatures and densities.

TABLE XI. Ratio of the stellar ^{134}Ba and ^{136}Ba cross sections and correlated uncertainties.

Thermal energy (keV)	Cross section ratio
10	2.70 ± 5.6%
12	2.72 ± 4.7%
20	2.78 ± 3.1%
25	2.82 ± 2.7%
30	2.84 ± 2.5%
40	2.89 ± 2.2%
50	2.92 ± 2.1%
52	2.92 ± 2.1%
60	2.94 ± 2.1%
70	2.96 ± 2.1%
80	2.97 ± 2.2%
90	2.97 ± 2.3%
100	2.96 ± 2.5%

TABLE XII. Maxwellian averaged neutron capture cross sections at $kT = 30$ keV compared to previous evaluations.

Isotope	$\langle\sigma v\rangle/v_T$ (mb)		
	This work	Bao and Käppeler [20]	Beer, Voss, and Winters [11]
^{134}Ba	176.3 ± 5.6	221 ± 35	221 ± 34
^{135}Ba	455.0 ± 15.0	457 ± 80	295 ± 59
^{136}Ba	62.0 ± 2.1	69 ± 10	60 ± 10
^{137}Ba	76.9 ± 2.9	57 ± 10	52 ± 10

VII. ASTROPHYSICAL IMPLICATIONS

A. Normalization of the $N_s\langle\sigma\rangle$ curve

The s-process reaction flow from iron to bismuth is described by the product of the produced s abundances and the respective cross sections of all involved isotopes. This quantity is characteristic for the s process, since it reflects the correlation $N_s \sim \langle\sigma\rangle^{-1}$ that follows from the fact that the neutron capture rates are practically independent of temperature in typical s-process environments. In the classical approach, the s-process abundances of neighboring isotopes are connected by a simple iterative expression [2],

$$(\sigma N_s)_A = \zeta_A (\sigma N_s)_{A-1}, \tag{2}$$

with

$$\zeta_A = \left(1 + \frac{1}{\sigma_A \tau_0}\right)^{-1}, \tag{3}$$

where A denotes the mass number and τ_0 the mean neutron exposure (see below). If plotted versus mass number, the resulting $N_s\langle\sigma\rangle$ curve can be fitted to the empirical $N_s\langle\sigma\rangle$ products of those s-only isotopes, which are not affected by branchings, and hence experience the entire reaction flow. The corresponding fit parameters yield information on the neutron economy during the s process (seed abundance and mean neutron exposure), while the $N_s\langle\sigma\rangle$ values correspond directly to the s abundances [2].

Among the normalization points of the $N_s\langle\sigma\rangle$ curve, ^{136}Ba is important because it is situated close to the neutron magic nuclei with $N = 82$, thus defining the turn-off point where the $N_s\langle\sigma\rangle$ curve exhibits a steplike decrease due to the small cross sections of the neutron magic nuclei. Together with the previously studied cases, ^{124}Te and ^{150}Sm, ^{136}Ba is expected to represent a further test of the s-process concept based on the classical approach. So far, this model has been surprisingly successful despite the extremely simple scenario, which assumes constant neutron density and temperature. In the following study, the currently best parameter set for the classical model was adopted from Ref. [6]: an exponential distribution of neutron exposures $\rho(\tau) \sim \exp(-\tau/\tau_0)$ with a mean value of $\tau_0 = 0.295$ mb^{-1} at a thermal energy of $kT = 29$ keV. The mean neutron density $n_n = (3.8 \pm 0.6) \times 10^8$ cm^{-3} was taken from Ref. [5].

Figure 7 shows the $N_s\langle\sigma\rangle$ curve calculated with the code SPEED.CLAS [43] in the mass region $120 < A < 155$. The empirical $N_s\langle\sigma\rangle$ values of the respective s-only isotopes are given for comparison. While all normalization points are in reasonable agreement with the calculated curve, ^{136}Ba falls short by 22%, which means that ^{136}Ba is overproduced in the model by this amount. Since the $N_s\langle\sigma\rangle$ curve is a continuously decreasing function of mass number, there is no way to readjust the fit in order to satisfy the ^{136}Ba point without creating a systematic discrepancy for all the heavier s isotopes.

An acceptable reason for an s-only isotope to fall below the calculated $N_s\langle\sigma\rangle$ curve could be that this isotope is partly bypassed in the s process due to a branching as it holds for ^{134}Ba (Fig. 1). However, this possibility can be excluded for ^{136}Ba because of the short half-life of the only possible branch point ^{136}Cs. The only other plausible explanation were then that the observed barium abundance may be too small. The meteoritic abundances given in recent compilations are $N_{Ba}^{\odot}$=4.49±0.28 [44] and 4.61±0.23 [45] relative to Si≡10^6, whereas the present data would suggest a 20% higher value of 5.50. This change would be in agreement with a recent abundance determination from the solar photosphere [46]. On the other hand, barium belongs to the group of refractory elements which show a rather consistent abundance pattern.

Possible p-process contributions to the s isotopes ^{134}Ba and ^{136}Ba were estimated by means of the p-process

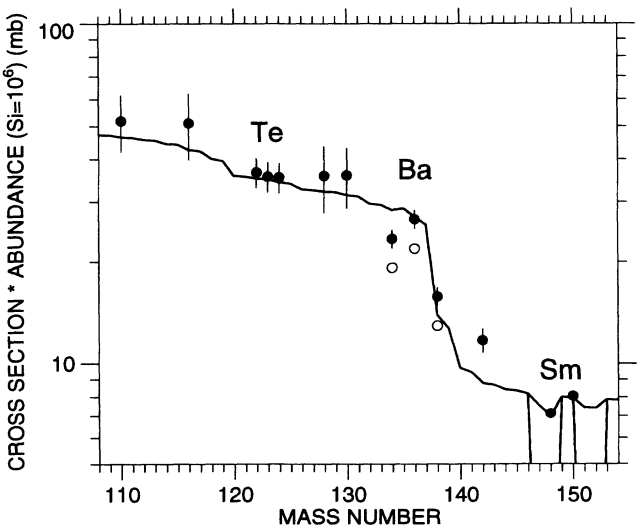

FIG. 7. The $N_s\langle\sigma\rangle$ curve calculated with the code SPEED.CLAS in the mass region $120 < A < 155$ in comparison to the empirical $N_s\langle\sigma\rangle$ values.

yields calculated by Howard, Meyer, and Woosley [47] and by Prantzos *et al.* [48]. On average, the suggested p contributions were 2% and <0.5% for ^{134}Ba and ^{136}Ba, respectively. This effect may influence the s-abundance ratio of ^{134}Ba and ^{136}Ba and should, therefore, be considered in a refined analysis of the ^{134}Cs branching. The absolute p contribution to ^{136}Ba has no impact on the renormalization of the barium abundance and was neglected.

The discrepancy between the meteoritic barium abundance and the abundance obtained with the classical approach is an important result and deserves further investigation: If the lower meteoritic abundance is correct, the barium problem would reveal the first true inconsistency of the classical approach. This would then imply that (a) more sophisticated s-process scenario(s) would be definitely required by the nuclear physics data themselves.

Presently, the only alternative to the classical approach for quantitative s-process calculations in this mass region is the model for helium shell burning in low mass AGB stars [49–51], which was also shown to reproduce the observed abundances rather well [6]. If this model is used with the latest input profiles for temperature and neutron density [52], the same 20% overproduction is obtained for ^{136}Ba as in the classical approach.

In the stellar model, however, neutron density and temperature are no longer constant. By far most of the neutron exposure occurs at significantly lower temperature (kT = 12 keV), followed by a comparably short neutron burst at kT = 26 keV. Normally, this second burst of neutrons does not affect the before produced abundance distribution because most neutron capture rates do not depend on temperature. However, this can be different at or near magic neutron numbers, where the level spacings are large. Accordingly, the cross section at low neutron energies exhibit a pronounced resonance structure, which can result in significant departures from the usual $1/v$ behavior of the cross section shapes. A striking example for such a case was recently reported by Beer *et al.* [22], who found a 50% enhancement in the 12 keV cross section of ^{138}Ba compared to the extrapolated $1/v$ shape.

Though the available information on resolved resonances was considered in evaluating the present Maxwellian average cross sections, it cannot be excluded that this part has been underestimated due to missing resonances. In fact, one finds that the overproduction of ^{136}Ba can be removed, if the cross section is artificially enhanced by 30% during the main neutron burst at kT = 12 keV.

In view of this problem, complementary cross section measurements at low energies are urgently needed for achieving a satisfactory interpretation of the observed barium abundance pattern.

B. The s-process branching at ^{134}Cs

The neutron capture flow through the Xe-Cs-Ba isotopes (Fig. 1) exhibits branchings at ^{133}Xe, ^{134}Cs, and ^{135}Cs. For all of these cases, the stellar β-decay rates differ from the respective laboratory rates [53], but only ^{134}Cs acts as a true branching point with significant competition between β decay and neutron capture. For ^{133}Xe, the neutron capture probability remains less than 0.5%, and ^{135}Cs affects the s-process flow only marginally, since its stellar half-life is still long compared to the time scale of the s process. The electron capture branch in the decay of ^{134}Cs is always less than 10^{-3} and can, therefore, be neglected.

The temperature dependence of the ^{134}Cs decay makes this branching a potential s-process thermometer. With the present results for the (n,γ) cross sections of ^{134}Ba and ^{136}Ba this thermometer can be analyzed for the first time in a quantitative way. The following discussion is based on the classical s-process approach [2]. In addition to the barium cross sections described above, the stellar cross sections for the Cs and Xe isotopes in Fig. 1, including the unstable branch point nuclei, are from Ref. [20].

With these data, the branching factor

$$f_n = \frac{\lambda_n}{\lambda_n + \lambda_\beta} \tag{4}$$

is defined in terms of the β-decay rate, $\lambda_\beta = \ln 2/t_{1/2}$, and the neutron capture rate, $\lambda_n = n_n \sigma v_T$ for the effective branch point ^{134}Cs. [σ is the stellar (n,γ) cross section and v_T the mean thermal neutron velocity.] The temperature dependence of the branching factor is shown in Fig. 8. The shaded band is obtained for the standard input data quoted above. The difference between upper and lower bound reflects the uncertainty in the neutron

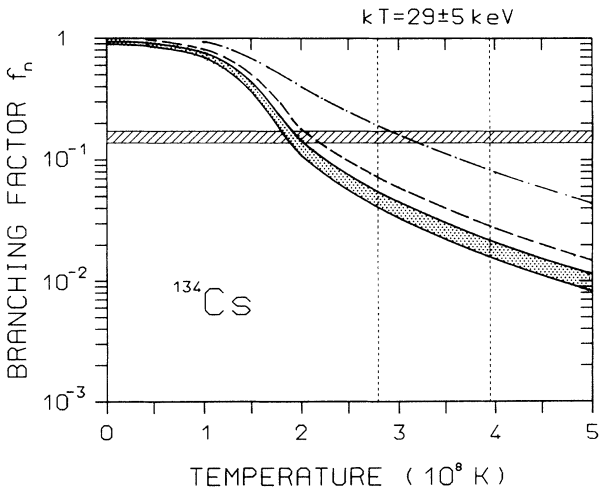

FIG. 8. The branching factor f_n for the s-process flow at ^{134}Cs. The dashed bar indicates the *effective* branching factor deduced from the $N_s\langle\sigma\rangle$ values of the s-only isotopes ^{134}Ba and ^{136}Ba. The temperature dependence was calculated assuming the standard parameters described in the text (shaded band) and with a modified cross section or β-decay rate for ^{134}Cs (dashed and dash-dotted lines, respectively). The temperature range obtained from other s-process thermometers [6] is shown by the vertical lines.

TABLE XIII. Decomposition of isotopic Ba abundances.

Isotope	$N_\odot$		Classical approach		AGB stars[a]
	Ref. [44]	N_{Ba}[b]	N_s[c]	$N_r = N_\odot - N_s$[d]	N_s[c]
^{134}Ba	0.109	0.133	0.157		0.147
^{135}Ba	0.296	0.362	0.064	0.298±0.023	0.055
^{136}Ba	0.353	0.432	0.432		0.439
^{137}Ba	0.504	0.617	0.334	0.283±0.040	0.372
^{138}Ba	3.22	3.941	3.716	0.225±0.372	3.590
Ba_{tot}		5.50	4.70		4.60

[a]For details, see text.
[b]Barium abundances renormalized to satisfy $N_\odot(^{136}Ba)=N_s$.
[c]Normalized at ^{124}Te.
[d]Uncertainties include the contributions from $N_\odot$ (±6.3%) and from N_s (typically ±4%, but ±7.5% for ^{138}Ba).

density only. The dashed line is obtained if the ^{134}Cs cross section is increased by 50%, corresponding to an optimistic estimate for the respective uncertainty. An even stronger effect is caused by the stellar β-decay rate of ^{134}Cs, which could be uncertain by a factor of 3 (dash-dotted line) [53].

The *effective* branching factor (dashed horizontal bar in Fig. 8) can be deduced via the s-only isotopes: Since ^{134}Ba is partially bypassed, while ^{136}Ba experiences the total flow, the branching factor can be calculated as

$$f_n = 1 - \frac{\zeta_{^{135}Ba}\zeta_{^{136}Ba}(\sigma N_s)_{^{134}Ba}}{(\sigma N_s)_{^{136}Ba}} = 0.176 \pm 0.025. \quad (5)$$

The quoted uncertainty originates from the uncertainty in the cross section ratio of ^{134}Ba and ^{136}Ba, since the ratio of the isotopic abundances is known within ±0.5% [54]. Note, that this discussion is based on the assumption that the relative s-process yields of the barium isotopes are not affected by the problem of the solar barium abundance discussed above.

Comparison of the *effective* branching factor with the calculated dependences in Fig. 8 shows that the standard parameters suggest a mean thermal energy, $kT_s \sim 16$ keV ($T_8 = 1.9$). This value is about 10% higher if the ^{134}Cs cross section is increased by 50%, but agreement with the plausible s-process range, $kT_s = 29\pm5$ keV (deduced from the analysis of the branchings at ^{151}Sm, ^{154}Eu, and ^{175}Lu [6]) is only achieved when the decay rate of ^{134}Cs is reduced by a factor of 3. This uncertainty is still within the limits estimated by Ref. [53].

If this branching is treated in the frame of the stellar model for helium shell burning in low mass stars, one obtains a similar result. It turns out that the calculated branching factor is also too small, accounting only for 40% of the effective value derived via Eq. (5).

In this situation, further studies have to concentrate on the improvement of the stellar β-decay rate of ^{134}Cs. However, an experimental determination seems presently out of reach, since this decay is enhanced via allowed transitions from thermally populated states to *excited* states in ^{134}Ba. Clearly, also the ^{134}Cs cross section needs to be improved. The statistical model calculations with *global* parameter systematics used so far may well exhibit much larger uncertainties than admitted above, particularly near closed neutron shells. In this respect, a measurement of the ^{135}Cs cross section [55] will be most helpful to build a *local* parameter systematics that is predominantly based on experimental data.

C. Decomposition into s- and r-process contributions

Because of the small isotopic (n,γ) cross sections, the abundance of the element barium is dominated by the s process. This makes it an important s-process indicator for astronomical observations related to studies of AGB stars and of problems related to the chemical evolution of the galaxy. With the improved cross sections presented here the s-process yields can be significantly better defined, resulting in a more reliable separation of s- and r-process abundances.

Compared with the meteoritic abundances (column 2 of Table XIII), the s-process yields of all even isotopes are significantly overproduced with the classical approach. In order to avoid overproduction, the barium

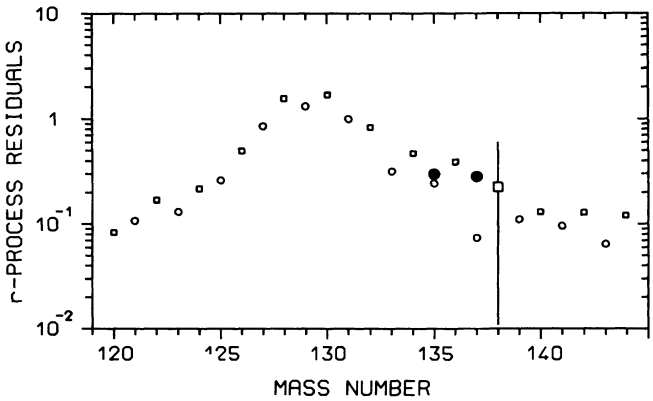

FIG. 9. The r-process abundance peak at mass number $A = 130$. Values from the present analysis are indicated by filled symbols, open symbols refer to the results of Refs. [2] and [57]. With the new results, the uncertainties could be reduced up to a factor of 4 and are now comparable to the size of the symbols. The large uncertainty for ^{138}Ba results from the fact that the r contribution is only a small fraction of the solar abundance.

TABLE XIV. (n,γ) Data for the interpretation of isotopic anomalies.

Isotope	GRB93[a] / BVW92	GRB93corrected for $N_{\odot,Ba}$=5.50 / BVW92	Present data / BVW92
^{134}Ba	1	0.82	0.80
^{135}Ba	1.8	1.48	1.54
^{136}Ba	1.3	1.07	1.03
^{137}Ba	2.2	1.80	1.48

[a]Gallino, Raiteri, and Busso [10]; Beer, Voss, and Winters [11].

abundance was normalized by a factor 1.22 such that $N_\odot(^{136}\text{Ba})=N_s(^{136}\text{Ba})$ (column 3). The decomposition into s and r abundances calculated from these modified abundances (column 5) is plotted in Fig. 9 together with the overall r distribution [2,56]. With the present data, the uncertainties in the r residuals could now also be reduced at the high energy tail of the r-process peak at $A = 130$, after the mass region between $A = 120$ and 126 had been improved recently [56]. The most significant difference compared to the decomposition of Ref. [2] was obtained for ^{137}Ba where the previous uncertainty was 4 times larger. In general, the new values fit better to a smooth distribution at the tail of the r-process peak.

The s-process yields obtained with the AGB model (column 6 in Table XIII) are rather similar to the results from the classical approach, but exhibit some differences, which exceed the respective cross section uncertainties, in particular for ^{134}Ba and ^{135}Ba. These differences are due to the different temperature profile of the AGB model (see Sec. VII B). As far as the r-process residuals are concerned, there is a difference with respect to ^{138}Ba, where the (lower) value derived with the classical approach seems to fit better to a smooth r distribution (Fig. 9).

The bottom line of Table XIII shows the sum over the isotopic barium abundances including the p nuclei ^{130}Ba and ^{132}Ba. Obviously, the calculations with the classical approach and with the AGB model agree that barium is mostly produced by the s process with an r-process admixture of only 15±6%. This result is related to the galactic chemical evolution and to the question whether the s process is a primary process, the respective yields being independent of stellar metallicity. (For a more detailed discussion see Pagel [12] and Magain and Zhao [57].)

D. Isotopic anomalies

Very large isotopic anomalies have been discovered in SiC grains of the Murchison meteorite for a number of elements, including xenon, barium, neodymium, and samarium. Among those, the barium anomalies are the best analyzed [7–9]. An astrophysical interpretation of these anomalies was presented by Gallino, Raiteri, and Busso (GRB furtheron) [10] in terms of a detailed model of He shell burning in thermally pulsing AGB stars. This analysis was based primarily on the cross section compilation of Beer, Voss, and Winters [11], but the authors note that the calculated barium abundance pattern did neither fit to the solar abundances nor to the observed anomalies. In view of the large uncertainties in the compiled data (see also Table XII), GRB tried to find a set of cross sections, by which they could explain the solar abundances and the anomalies as well. Table XIV summarizes this situation: Column 2 lists the ratios of adopted and compiled cross sections required for an s-process origin of the isotopic anomalies in barium [10]. With the renormalized barium abundance, these factors reduce to the values in column 3, which are—in fact—very close to the ratios obtained from the present results. This means that the new data represent not only an improved basis for analyzing the barium anomalies, but that these anomalies may be naturally explained as being due to s-processed material.

ACKNOWLEDGMENTS

We would like to thank the many colleagues of KfK who contributed to this work. In particular, we are indebted to Ch. Adelhelm, E. Nold, and M. Mackert from the Institute of Material Research for analyzing the water content of the samples and for converting the barium nitrate into carbonate, as well as for the spontaneous help of E. Gantner, H. Deutsch, and H. Klewe-Nebenius from the Institute of Radiochemistry, who determined the isotopic compositions. We have to thank F.H. Fröhner and B. Krieg from the Institute of Neutron Research and Reactor Technology for providing the JEF data, and H. Ottmar and H. Eberle for analyzing the samples by K x-ray absorptiometry. Last but not least, these measurements were possible only with the continuous support of the Van de Graaff crew, D. Roller, E.-P. Knaetsch, and W. Seith who ran the accelerator in a most efficient way, and of G. Rupp, who was untiring in optimizing the experimental setup. We also thank Zs. Németh from the KFKI Budapest for pointing out the possibility to derive isomeric ratios from the present data.

[1] K. Wisshak, K. Guber, F. Käppeler, J. Krisch, H. Müller, G. Rupp, and F. Voss, Nucl. Instrum. Methods Phys. Res. Sect. A **292**, 595 (1990).

[2] F. Käppeler, H. Beer, and K. Wisshak, Rep. Prog. Phys. **52**, 945 (1989).

[3] K. Wisshak, F. Voss, F. Käppeler, and G. Reffo, Phys. Rev. C **45**, 2470 (1992).

[4] D. D. Clayton, W. A. Fowler, T. E. Hull, and B. A.

Zimmerman, Ann. Phys. **12**, 331 (1961).
[5] K. Wisshak, K. Guber, F. Voss, F. Käppeler, and G. Reffo, Phys. Rev. C **48**, 1401 (1993).
[6] F. Käppeler, R. Gallino, M. Busso, G. Picchio, and C. Raiteri, Astrophys. J. **354**, 630 (1990).
[7] U. Ott and F. Begemann, Astrophys. J. **353**, L57 (1990).
[8] E. Zinner, S. Amari, and R. S. Lewis, Astrophys. J. **382**, L47 (1991).
[9] F. A. Prombo, S. Podosek, S. Amari, and R. S. Lewis, Astrophys. J. **410**, 393 (1993).
[10] R. Gallino, C. M. Raiteri, and M. Busso, Astrophys. J. **410**, 400 (1993).
[11] H. Beer, F. Voss, and R. R. Winters, Astrophys. J. Suppl. **80**, 403 (1992).
[12] B. E. J. Pagel, Rev. Mexicana Astron. Astrof. **18**, 161 (1989).
[13] D. L. Lambert, in *Cosmic Abundances of Matter*, edited by C. J. Waddington (AIP, New York, 1989), p. 168.
[14] B. S. Meyer, G. J. Mathews, W. M. Howard, S. E. Woosley, and R. D. Hoffman, Astrophys. J. **399**, 656 (1992).
[15] A. R. de L. Musgrove, B. J. Allen, and R. L. Macklin, Technical report, Australian Atomic Energy Commission (unpublished).
[16] A. R. de L. Musgrove, B. J. Allen, J. W. Boldeman, and R. L. Macklin, Nucl. Phys. **A256**, 173 (1976).
[17] A. R. de L. Musgrove, B. J. Allen, J. W. Boldeman, and R. L. Macklin, Aust. J. Phys. **29**, 157 (1976).
[18] A. R. de L. Musgrove, B. J. Allen, J. W. Boldeman, and R. L. Macklin, in *Neutron Physics and Nuclear Data for Reactors and Other Applied Purposes* (OECD, Paris, 1978), p. 449.
[19] B. J. Allen, J. W. Boldeman, and R. L. Macklin, Nucl. Sci. Eng. **82**, 230 (1982).
[20] Z. Y. Bao and F. Käppeler, At. Data Nucl. Data Tables **36**, 411 (1987).
[21] M. Mizumoto, M. Sugimoto, M. Ohkubo, Y. Nakajima, Y. Furuta, and Y. Kawarasaki, in *Nuclear Data for Basic and Applied Science* (Gordon and Breach, New York, 1986), p. 533.
[22] H. Beer, F. Corvi, A. Mauri, and K. Athanassopulos, in *Nuclei in the Cosmos*, edited by F. Käppeler and K. Wisshak (IOP, Bristol, 1993), p. 227.
[23] F. Voss, K. Wisshak, K. Guber, F. Käppeler, and G. Reffo, Report No. KfK–5253, Kernforschungszentrum Karlsruhe, 1994.
[24] K. Wisshak, F. Voss, F. Käppeler, and G. Reffo, Phys. Rev. C **42**, 1731 (1990).
[25] K. Guber, Ph.D. thesis, University of Karlsruhe, 1993.
[26] G. Winkler, Nucl. Instrum. Methods Phys. Res. Sect. A **282**, 317 (1989).
[27] H. Ottmar *et al.*, in *Proceedings of an International Symposium on Nuclear Material Safeguards* (IAEA, Vienna, 1987), p. 201.
[28] R. de Meester, H. Eberle, S. Johnson, L. Koch, I. Michel–Piper, H. Nackaerts, and H. Ottmar, in [27], p. 233.
[29] C. Nordborg, H. Gruppelaar, and M. Salvatores, in *Nuclear Data for Science and Technology*, edited by S. Qaim (Springer, Berlin, 1992), p. 782.
[30] V. McLane, C. L. Dunford, and P. F. Rose, in *Neutron Cross Sections* (Academic Press, New York, 1988), Vol. 2.
[31] A. V. Murzin, private communication (unpublished).
[32] F. H. Fröhner, technical report, Kernforschungszentrum Karlsruhe (unpublished).
[33] G. Reffo, F. Fabbri, K. Wisshak, and F. Käppeler, Nucl. Sci. Eng. **80**, 630 (1982).
[34] K. Wisshak, F. Käppeler, and G. Schatz, Nucl. Instrum. Methods **221**, 385 (1984).
[35] N. Weber, diplom thesis, University of Karlsruhe, 1993.
[36] F. H. Fröhner, Technical report, Gulf General Atomic (unpublished).
[37] J. F. Mughabghab, M. Divadeenam, and N. E. Holden, in *Neutron Cross Sections* (Academic Press, New York, 1981), Vol. 1, Part A.
[38] R. L. Macklin, private communication (unpublished).
[39] W. Ratynski and F. Käppeler, Phys. Rev. C **37**, 595 (1988).
[40] F. Corvi, A. Prevignano, H. Liskien, and P. B. Smith, Nucl. Instrum. Methods Phys. Res. Sect. A **265**, 475 (1988).
[41] J. A. Holmes, S. E. Woosley, W. A. Fowler, and B. A. Zimmerman, At. Data Nucl. Data Tables **18**, 305 (1976).
[42] M. J. Harris, Astrophys. Space Sci. **77**, 357 (1981).
[43] H. Beer, technical report, Kernforschungszentrum Karlsruhe (unpublished).
[44] E. Anders and N. Grevesse, Geochim. Cosmochim. Acta **53**, 197 (1989).
[45] H. Palme and H. Beer, in *Landolt–Börnstein New Series, Vol. VI/3a*, edited by O. Madelung (Springer, Berlin, 1993), p. 196.
[46] P. Magain, private communication (unpublished).
[47] W. Howard, B. Meyer, and S. Woosley, Astrophys. J. **373**, L5 (1991).
[48] N. Prantzos, M. Hashimoto, M. Rayet, and M. Arnould, Astron. Astrophys. **238**, 455 (1990).
[49] D. E. Hollowell and I. Iben Jr., Astrophys. J. **333**, L25 (1988).
[50] D. E. Hollowell and I. Iben Jr., Astrophys. J. **340**, 966 (1989).
[51] R. Gallino, M. Busso, G. Picchio, and C. Raiteri, Astrophys. J. **334**, L45 (1988).
[52] R. Gallino, private communication (unpublished).
[53] K. Takahashi and K. Yokoi, At. Data Nucl. Data Tables **36**, 375 (1987).
[54] J. De Laeter, private communication (unpublished).
[55] F. Käppeler, M. Wiescher, and P. E. Koehler, in *Workshop on the Production and Use of Intense Radioactive Beams at the Isospin Laboratory*, edited by J. D. Garrett (Joint Institute for Heavy Ion Research, Oak Ridge, TN, 1992), p. 163.
[56] F. Käppeler, W. Schanz, K. Wisshak, and G. Reffo, Astrophys. J. **410**, 370 (1993).
[57] P. Magain and G. Zhao, Astron. Astrophys. **268**, L27 (1993).

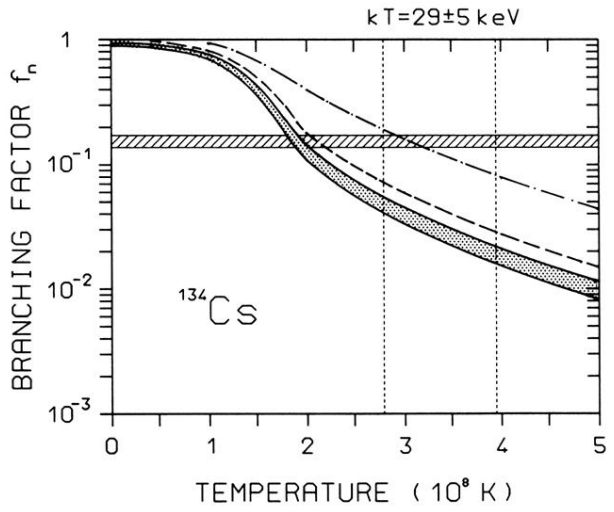

FIG. 8. The branching factor f_n for the s-process flow at ^{134}Cs. The dashed bar indicates the *effective* branching factor deduced from the $N_s\langle\sigma\rangle$ values of the s-only isotopes ^{134}Ba and ^{136}Ba. The temperature dependence was calculated assuming the standard parameters described in the text (shaded band) and with a modified cross section or β-decay rate for ^{134}Cs (dashed and dash-dotted lines, respectively). The temperature range obtained from other s-process thermometers [6] is shown by the vertical lines.